REPORT DOCUMENTATION PAGE

AFRL-SR-AR-TR-04-

0567

PLEASE DO NOT RETURN YOUR FORM TO THE ABOVE ADDRESS.

1. REPORT DATE (DD-MM-YYYY)	2. REPORT DATE	3. DATES COVERED (From - To)
11-00-2004		8/1/02-7/31/03

4. TITLE AND SUBTITLE
An All-Optical Silicon Nano-Transistor

5a. CONTRACT NUMBER
FA9550

5b. GRANT NUMBER
F49620-02-1-0396

5c. PROGRAM ELEMENT NUMBER
AFOSR/PK1

6. AUTHOR(S)
Michal Lipson

5d. PROJECT NUMBER
4B578

5e. TASK NUMBER

5f. WORK UNIT NUMBER
12.910

7. PERFORMING ORGANIZATION NAME(S) AND ADDRESS(ES)
Cornell University
Electrical and Computer Engineering
411 Phillips Hall
Ithaca New york, 14850, USA

8. PERFORMING ORGANIZATION REPORT NUMBER

9. SPONSORING/MONITORING AGENCY NAME(S) AND ADDRESS(ES)

10. SPONSOR/MONITOR'S ACRONYM(S)
AFRL

11. SPONSORING/MONITORING AGENCY REPORT NUMBER
10 U.S.C 2358

12. DISTRIBUTION AVAILABILITY STATEMENT
Distribution Statement A: unlimited

13. SUPPLEMENTARY NOTES

20041112 030

14. ABSTRACT
We provide Silicon with optoelectronic capabilities using highly confined photonic structures. The photonic structures enhance the free carrier injection effect on the Silicon index of refraction, by orders of magnitude. We present experimental demonstration of fast all-optical switching on a silicon photonic integrated device by employing a strong light-confinement structure to enhance sensitivity to small changes in the refractive index. By use of a control light pulse with energy as low as 40 pJ, the optical transmission of the structure is modulated by more than 97% with a time response of 450 ps. We also demonstrate a 20-μm-long tunable optical resonator integrated on a silicon-on-insulator waveguide. The microresonator consists of a planar Fabry–Pérot microcavity defined by deep Si/SiO2 Bragg reflectors with a high finesse of 11.2. The device is electrically driven and shows a modulation depth as high as 53% for a power consumption of only 20 mW. The results could enable an all-optical CMOS compatible chip, where all of the devices would be monolithically grown on-chip.

15. SUBJECT TERMS

16. SECURITY CLASSIFICATION OF:			17. LIMITATION OF ABSTRACT	18. NUMBER OF PAGES	19a. NAME OF RESPONSIBLE PERSON
a. REPORT	b. ABSTRACT	c. THIS PAGE			19b. TELEPONE NUMBER (Include area code)

Contents

ORIGINAL RESEARCH PROPOSAL SUMMARY

STATEMENT OF WORK

In this proposal I will develop Silicon optically active components (such as tunable filters, switches and modulators) and, in particular, an all-optical transistor. One could then envision an **all-optical CMOS compatible chip,** where all of the devices would be monolithically grown on-chip.

I intend to provide Silicon with optoelectronic capabilities using photonic crystals. Photonic crystals can enhance light-matter interaction, **enhancing the free carrier injection effect on the Silicon index of refraction,** by orders of magnitude.

The first stage of the work will be to **achieve a low-loss Si waveguiding platform.** The main focus will in achieving single mode waveguides with low propagation losses (<1dB/cm). This stage will consist in designing, fabricating and characterizing the structures. The second stage of the work will be to **achieve a nm-size strong light confining structure**. This will be done by designing a planar Si microcavity, fabricating and characterizing the structure. The focus here will be given in achieving high Q (100-1000) structures. The third stage of the work will be to **build the final all-optical transistor.** This will require the demonstration of tuning of a microcavity spectral response with optical pumping, followed by the design and fabrication of the optical transistor. The fourth and final stage will consist in **characterizing the transistor**. This will consist of pump-probe experiments to determine switching speed, degree of switching and required pump intensity. An additional optional stage will consist in achieving an all-optical transistor for both pump and probe operating at 15 microns, this is extremely important for all-optical computing and signal processing. This stage will consist of Z-scan measurements on a Si microcavity.

DELIVERABLES

The results of this research will open the door to a new field, where manipulation of light on a Silicon chip is possible and will provide the basic building block for an all-optical CMOS chip. The deliverable physical devices of this research are:

- Strong light confining Si planar cavity

The structure will be scalable with wavelength. Such a cavity is extremely important for any applications that require strong light intensity operation, such as lasers, amplifiers, etc. The expected degree of light confinement Q is between 100 and 1000. The total length of the structure is between 10 and 100μm, while the cavity is 10-100nm long.

- A Si all-optical transistor

Operating at 1.5μm. Total switching capability with psec time response is expected. The total length of the structure is between 10 and 100μm. The relationship between the different parameters such as photonic crystal geometry, pumping intensity, wavelength of operation and switching speed will be given, so that the device can be scalable with wavelength and used for different speed and pump intensity requirements.

As a result of this research I expect to achieve a better understanding of:

- Silicon optical processes such as the dynamics of free carrier injection and its effect on the index of refraction

- Physical processes in strong light confinement in photonic crystals and their effect on enhancing light-matter interaction
- Critical nanofabrication processes for achieving high quality photonic structures

All of the results of the research will be disseminated through scientific publications

TECHNICAL REPORT

External control of light on Silicon for switching and modulating

We have done work on both electro-optical and all-optical modulators and switches. Both devices are based on free carrier injection for modulating the index of refraction of Silicon. The work on the electro-optical switches, demonstrating the benefits f using highly confined structure for enhancing the effect of the index modulation, enabled the all-optical devices.

Below I describe Silicon structures for chip-scale modulators and switches. Modulators usually encode signals, while switches route signals. The difference between modulators and switches in the context of the proposed research lies in the speed, modulation depth and geometry. For switches, high modulation depth is crucial and usually devices with at least three ports are necessary. For modulators, high speed is crucial and devices with two ports are usually sufficient. In this section I describe the building blocks common for both switching and modulating.

Electro-optic devices

To date most of the work done on active devices on Silicon is based on MEMS (Micro-electro-mechanical systems) technology. One of the main drawbacks with MEMS is their slow response, with switching speeds of about 1-100 ms. Optical modulation can also be done using the thermo-optic effect in Silicon. The thermo-optic coefficient for silicon is typically 3 times greater than in classical thermo-optical materials and 8 times greater than in silica-based materials. The effect, however, is rather slow and can only be used for up to 1 MHz modulation frequencies [**Error! Reference source not found.**].

Year	Author	Electrical structure	Optical structure	M (%)	J (kA/cm^2)	Power (mW)	t_s, ns	Length (μm)	Dem./Prop.
1987	Lorenzo et al. [2]	p-i-n	Cross switch	50	1.26	-	-	2000	D
1989	Hemenway et al. [3]	p-i-n	Mach-Zehnder	30	100.0	-	18	v.d.	D
1991	Treyz et al. [4]	p-i-n	FCAM	75	3.0	-	50	500	D
1991	Treyz et al [5]	p-i-n	Mach-Zehnder	65	1.6	-	<50	500	D
1991	Xiao et al. [6]	p-i-n	F-P	10	6.0	-	25	v.d.	D
1994	Liu et al. [7]	p-i-n	Y-switch	>90	9.0	-	200	800	D
1994	Liu et al. [8]	p-i-n	TIR-switch	>90	12.5	-	100	200	D
1995	Zhao et al. [9]	p-i-n	Mach-Zehnder	98	-	-	200	816	D
1995	Liu et al. [10]	p-i-n	F-P	80	-	-	-	20.9	P
1996	Zhao et al .[11]	p-i-n	ZGDC	97.2	1.027	123.7	210	1103	D
1997	Cutolo et al. [12]	p-i-n	Bragg reflector	50	-	4	24.7	3200	P
1997	Cutolo et al. [13]	BMFET	FCAM	20	2.3	126	6	1000	P
1997	Zhao et al. [14]	p-i-n	TIR	>88	8.8	-	110	190	D
2001	Coppola et al. [15]	p-i-n	Bragg reflector	94	-	0.3	5	3200	P
2003	Sciuto et al. [16]	BMFET	FCAM	75	-	160	-	400	D
2003	**Barrios et al. [17]**	**p-i-n**	**F-P**	**80**	**0.116**	**0.025**	**21**	**20**	**P**
2003	Barrios et al. [18]	p-i-n	F-P	80	0.61	0.014	1.3	10	P

Table I. All-silicon electro-optic modulators reported in the literature (BMFET=Bipolar Mode Field-Effect Transistor; FCAM=Free Carrier Absorption Modulator; F-P=Fabry-Perot; TIR=Total Internal Reflection; ZGDC=Zero Gap Directional Coupler; M=amplitude modulation depth; J=current density; t_s=switching time; v.d.= vertical device; Dem.(D)=demonstrated; Prop.(P)=proposed).

An approach for faster modulation on Si is the electrical modulation of the refractive index in a specific region of planar optical devices such as Mach-Zehnder modulators, total-internal-reflection (TIR)-based structures, cross-switches, Y-switches and Fabry-

Perot (F-P) resonators (see Table I). The absence of mechanical elements in these devices makes them more reliable than MEMS. Table I shows that most of the listed devices present common features: long interaction distance and high injection current densities and power consumption in order to obtain a useful modulation depth. Most of the previously proposed Si electro-optic (E-O) switches, however, are long and require high drive powers. Such length and power requirements impose difficulties in integrating these devices on chip. There is therefore an urgent need for structures that can be implemented in a micron-size region offering low current density, low power consumption and high –modulation depth.

In [17] we consider a 1-D microcavity embedded in a ridge waveguide for optical switching. Highly confined optical microcavities enable the confinement and enhancement of the optical field in a very small region. The transmission of these

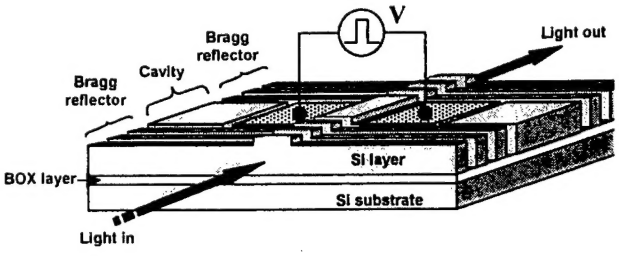

Fig. 1. 1-D microcavity in a Silicon ridge waveguide

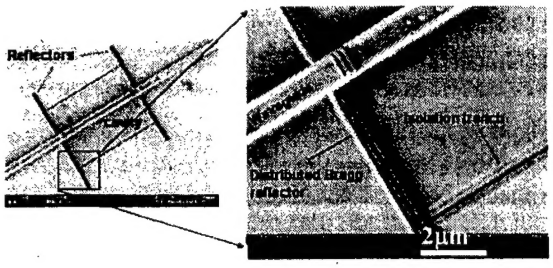

Fig. 2. SEM of the structure on the left

structures is highly sensitive to small index changes in the cavity, making them adequate for intensity modulation applications in a short length [18]. In addition, since the refractive index modulation can be confined to the cavity region, the electrical power to produce the desired phase change can be made very small. Fig. 1 shows a perspective schematic of the electro-optic modulator. For illustration purposes, the trenches down to the buried oxide (BOX) layer are drawn as empty. In our simulations these are assumed to be completely filled with SiO_2. The device consists of a F-P cavity formed by two DBRs in a SOI rib waveguide. Both DBRs consist of the same number of Si/SiO_2 periods down to the BOX layer. Two lateral trenches down to the BOX layer are on both sides of the rib for carrier confinement, in the region where the optical field is confined as well. Heavily doped p^+ and n^+ regions are defined in the cavity region, at both sides of the rib. Metal electrodes contact both the p^+ (anode) and n^+ (cathode) regions. Fig. 2 shows a fabricated device of the passive microcavity structure (no electrical contact). Our calculations show that a 20 μm long device is predicted to exhibit ~80% of modulation depth at 1.55 μm operation wavelength by using only ~25 μW of electrical power and a drive current density of 116 A/cm^2, leading to an increase of the device temperature $<10^{-2}$ K. The switching speed of this device is calculated to be ~16 ns, with no significant thermo-optic effect. The estimated dc power consumption for this device is at least one order of magnitude smaller than the smallest reported (theoretical) value [28]. These characteristics reveal the benefits of confining both the optical field and the injection carriers in the cavity region in order to improve the electro-optic modulator performance

in terms of power consumption, current density, device length, and modulation depth. These results show the principle of strong optical and electrical confinement for electro-optical switching with ultra-low power in a micron-size Si structure.

The principle of strong confinement of light and carriers, demonstrated in these results, will enable novel devices for electro-optic switches as well as modulators. The devices could include for example four port devices and devices based on embedded waveguides. Devices with different confinement levels, power dissipation and bandwidth could be tailored for different functionalities.

All-optical switching on a Si chip

All optical switching, i.e., controlling a probe beam with a pump beam, has been one of the holy grails in the area of photonics. It could open the door to ultra-fast circuits free of optic-to-electronic conversation, a main source of speed limitation in electro-optic devices. All-optical switching has been demonstrated in compound semiconductors [33]. In Silicon, however, ultra-fast all-optical switching has been demonstrated only for vertical structures using very high pumping powers with modest signal modulations [34-22].

In [23,24] we demonstrated all-optical modulation on a Si sub-micron-size planar structure. The modulator is based on a highly confining ring resonator. The advantage of the ring resonators is that a small change of index of refraction is sufficient for completely detuning the resonance. For a ring resonator of 10μm, an index change as small as 10^{-3} is sufficient to tune the resonance by 1 nm. We study ring resonators coupled to single waveguides (see Fig. 3). These ring resonators transmit signals with wavelengths that do not correspond to the resonances of the ring (see Fig. 4). The resonances of the ring can be tuned by modifying the index of refraction of the ring (or part of the ring) and therefore a modulation of the signal transmitted through the ring resonator can be achieved (see Fig. 5).

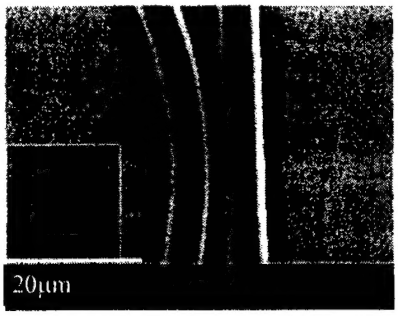

Fig. 3. Scanning electron micrograph of a detail of 10 μm diameter ring coupled to the waveguide. Inset shows the whole ring structure (scale bar applies to inset).

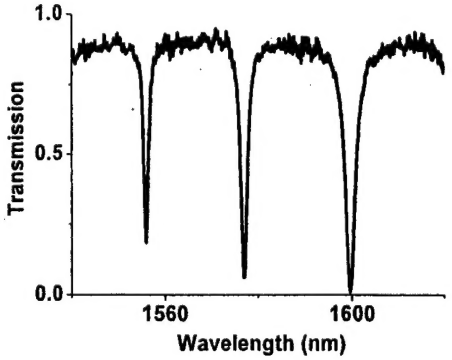

Fig. 4. Measured spectrum of the 10 μm ring-resonator seen in Fig.3.

Figure 3 shows a 10 μm diameter ring resonator. The inset shows the whole ring structure. The figure shows a zoom in of part of the ring coupled to the waveguide. The devices were patterned by electron-beam lithography and subsequently etched by ICP-RIE following the same process and simultaneously with the nano-taper coupler

described earlier. The spectral response of the fabricated device is shown in Fig. 4. One can see that the Q of the cavity is extremely high, demonstrating strong light confining in the structure, which in turn signifies strong dependence on the index of refraction of the ring.

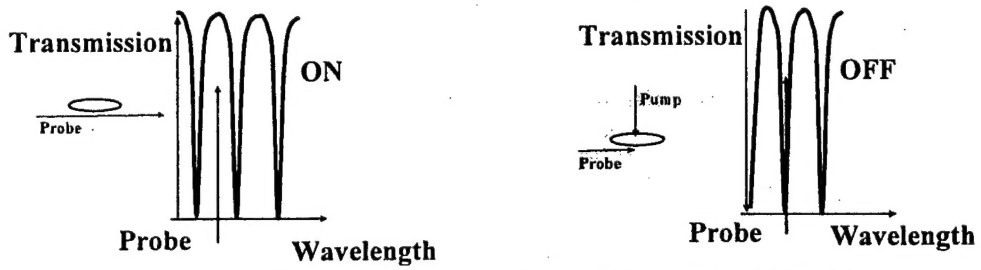

Fig. 5. Typical spectra of a switch in an ON and OFF state

In [23] a Titanium:Sapphire femtosecond laser is used to generate 120 fs pulses at λ_{laser} = 800 nm with 1.5 nJ energy and 80 MHz repetition rate. The femtosecond laser pulse is converted into the pump pulse at λ_{pump} = 400 nm through second-harmonic generation using a Beta-Barium-Borate (BBO) non-linear crystal. The pump pulse is focused onto the single-coupled Si ring resonators. The pump pulse energy is less than 120 pJ at the ring resonator plane, which corresponds to an average optical pump power of less than 10 mW. A probe CW beam is focused into the waveguide, which is coupled to the ring resonator and collected by a 5 GHz photodetector with nominal fall/rise times of about 70 ps.

In [24] two-photon absorption is used to generate the free carrier. In contrast to [23], both pump and probe beams are in the 1.5micron spectral range, and are both coupled in-plane. In [24] the laser source for the pump is a tunable mode-locked optical parametric oscillator (OPO), which in turn is pumped by a Ti:sapphire picosecond laser at a 78-MHz repetition rate. The OPO generates 1.5-ps pulses that pass through a Fabry-Perot tunable filter in order to produce the pump beam, which comprises 10-ps pulses with energy of less than 25-pJ coupled to the silicon waveguide input. A tunable continuous-wave laser provides the probe signal. Both pump and probe beams are set to be linearly polarized (quasi-TM) by use of independent polarization controllers. The pump and probe beams are combined by directional couplers and coupled into the silicon waveguide by an external tapered-lensed fiber and an on-chip fiber-to-waveguide nanotaper coupler17. The transmitted probe signal is coupled into a collimator and separated from the transmitted pump light through a band-pass tunable grating filter. The probe signal is detected by a high-speed DC-12GHz photodetector with a nominal fall/rise time of 30 ps. A 20-GHz digital sampling oscilloscope is used to record the probe signal.

The temporal response of the transmitted probe signals in [23] are shown in Fig. 6 for two distinct probe wavelengths: λ_{probe} = 1,554.6 nm (below resonance) and λ_{probe} = 1,555.5 nm (on resonance). Similar results were obtained in [24]. The measured modulation depth (*MD*) is defined as $MD = (I_{max} - I_{min}) / I_{max}$, where I_{max} and I_{min} are, respectively, the maximum and minimum probe optical power signal for a fixed wavelength. The modulation depth is about 75% for λ_{probe} = 1,554.6 nm and 97% for λ_{probe} = 1,555.5 nm. The measured modulation depth is limited only by the photodetector response time. For a photodetector with a response time of less than 20 ps, one should

expect to measure modulation depths of nearly 100% at both probe wavelengths.

By assuming an instantaneous spectral shift of the spectrum, followed by a simple exponential decay representing the free-carrier relaxation time, a wavelength peak shift of $\Delta\lambda$ = -1.1 nm and a relaxation time of τ_{fc} = 450 ps is btained. This relaxation time, much shorter than the bulk Si free-carrier lifetime, is not fundamental, and is due to fast recombination mechanisms on the unpassivated sidewalls of the structures. By manipulating the degree of surface passivation or by using ion implantation, the free-carrier lifetime could be further decreased. The wavelength peak shift of the ring resonator corresponds to an effective index change of $\Delta n_{eff} = -1.45 \cdot 10^{-3}$, or equivalently to a refractive index change in the silicon core of $\Delta n_{Si} = -1.6 \cdot 10^{-3}$. This refractive index change is caused by a free-carrier concentration of $\Delta N = \Delta P = 4.8 \cdot 10^{17}$ cm^{-3}. Considering the physical dimensions of the ring resonator, the optical pulse energy that needs to be absorbed by the ring resonator in order to excite such a free-carrier concentration is estimated to be of only 0.9 pJ. The losses due to absorption[3], estimated from free-carrier concentration are $\Delta\alpha$ = 6.9 cm^{-1}, significantly lower than the estimated scattering losses in the ring resonator of α_{ring} = 33.6 cm^{-1}. The relative low absorption losses indicate that the observed modulation is due only to a refractive index change and that thermal effects can be neglected. This is of foremost importance for the application of the proposed device as an all-optical gate, enabling near 100% transmission of the data signal once the gate is open.

These results form the basis for novel devices for all-optical Si modulators and switches, enabling entirely novel architectures on chip. Devices confining both pump and probe with different confinement levels would enable different functionalities. One could envision for example the pump light, externally coupled to the chip, being guided in SiO_2/air waveguides for modulating Si devices in specific locations on the chip.

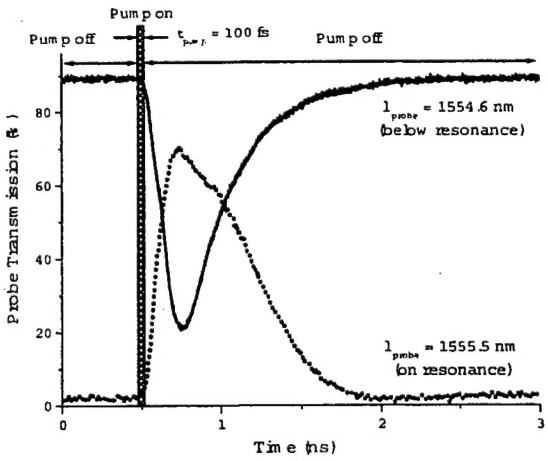

Fig. 6. Temporal response of the probe signal to the pump excitation showing transmission for probe wavelengths below resonance (solid line) and on resonance (dotted line).

Conclusion

Our recent results using sub-micron size highly confining structures in Si show the feasibility of switching and coupling light on-chip. These results form the building blocks

for all-optical circuits, where passive as well as active components could be integrated on a single chip. The demonstrated devices could form the basis for new on-chip and chip-to chip architectures for low power and high bandwidth applications.

Reference:

1 G. Cocorullo, M. Iodice and I. Rendina, "All-silicon Fabry-Perot modulator based on the termo-optic effect," Optics Letters, vol. 19, no.6, p.420, 1994.

2 J.P. Lorenzo and R.A. Soref, "1.3 μm electro-optic silicon switch," Appl. Phys. Lett., 51(1), p.6, 1987.

3 B.R. Hemenway, O. Solgaard, and D.M. Bloom, "All-silicon integrated optical modulator for 1.3 μm fiber-optic interconnects," Appl. Phys. Lett. 55(4), p. 349, 1989.

4 G.V. Treyz, P.G. May and J.-M. Halbout, "Silicon optical modulators at 1.3 μm based on free-carrier absorption," IEEE Electron Dev. Lett., vol 12, no. 6, p. 276, 1991

5 G.V. Treyz, P.G. May, and J.-M. Halbout, "Silicon Mach-Zehnder waveguide interferometers based on the plasma dispersion effect," Appl. Phys. Lett., 59 (7), p.771, 1991.

6 X. Xiao, J.C. Sturm, K.K. Goel, and P.V. Schwartz, "Fabry-Perot Optical Intensity Modulator at 1.3 μm in Silicon," IEEE Photon. Technol. Lett., vol.3 no. 3, p.230, 1991.

7 Y.L. Liu, E.K. Liu, S.L. Zhang, G.Z. Li and J.S. Luo, "Silicon 1x2 digital optical switch using plasma dispersion," Electron. Lett. Vol.30, no. 2, p.130, 1994.

8 Y. Liu, E. Liu, G. Li, S. Zhang, J. Luo, F. Zhou, M. Cheng, B. Li, and H. Ge, "Novel silicon waveguide switch based on total internal reflection," Appl. Phys. Lett., 64 (16), p. 2079, 1994.

9 C.Z. Zhao, G.Z. Li, E.K. Liu, Y. Gao, and X.D. Liu, "Silicon on insulator Mach-Zehnder waveguide interferometers operating at 1.3 μm," Appl. Phys. Lett., 67(17), p.2448, 1995.

10 M.Y. Liu and S. Chou, "High-modulation-depth and short-cavity-length silicon Fabry-Perot modulator with two grating Bragg reflectors," Appl. Phys. Lett. 68 (2), p.170, 1995.

11 C.Z. Zhao, E.K. Liu, G.Z. Li, Y. Gao, and C.S. Guo, "Zero-gap directional coupler switch integrated into a silicon-on-insulator for 1.3-μm operation," Optics Lett., vol.21, no.20, p.1664, 1996.

12 A. Cutolo, M. Iodice, A. Irace, P. Spirito, and L. Zeni, "An electrically controlled Bragg reflector integrated in a rib silicon on insulator waveguide," Appl. Phys. Lett., 71 (2), p.199, 1997.

13 A. Cutolo, M. Iodice, P. Spirito, and L. Zeni, "Silicon electro-optic modulator based on a three terminal device integrated in a low-loss single-mode SOI waveguide," J. Lightwave Technol., vol. 15, no. 3, p. 505, 1997.

14 C.Z. Zhao, A.H. Chen, E.K. Liu, and G.Z. Li, "Silicon-on-insulator asymmetric optical switch based on total internal reflection," IEEE Photon. Technol. Lett., vol. 9, no.8, p.1113, 1997.

15 G. Coppola, A. Irace, M. Iodice, and A. Cutolo, "Simulation and analysis of a high-efficiency silicon optoelectronic modulator based on a Bragg mirror," Opt. Eng. 40(6), 1076-1081 (2001).
16 A. Sciuto, S. Libertino, A. Alessandria, S. Coffa, and G. Coppola, "Design, fabrication, and testing of an integrated Si-based light modulator," J. Lightwave Technol., vol. 21, no. 1, p. 228, 2003.
17 C. Angulo Barrios, V. Almeida, and M. Lipson, "Low-power-consumption short-length and high-modulation-depth silicon electrooptic modulator," J. Lightwave Technol. vol 21, no.4, p.1089, April 2003
18 Barrios, C. A., Almeida, V. R., Panepucci, R. R., and M. Lipson, "Electro-optic Modulation of Silicon-on-insulator Submicron-size Waveguide Devices", IEEE Journal of Lightwave Technologies, 21, p. 2332, 2003.
19 Nan Chi ; Jianfeng Zhang ; Holm-Nielsen, P.V. ; Lin Xu ; Monroy, I.T. ; Peucheret, C. ; Yvind, K. ; Christiansen, L.J. ; Jeppesen, P. ,"Experimental demonstration of cascaded transmission and all-optical label swapping of orthogonal IM/FSK labelled signal", Electronics Letters 39, no. 8, (2003) : 676-8
20 Hache, A. ; Bourgeois, M. Ultrafast all-optical switching in a silicon-based photonic crystal, Applied Physics Letters 77, no. 25, (18 Dec. 2000) : 4089-91
21 Dinu, M. ; Quochi, F. ; Garcia, H. Third-order nonlinearities in silicon at telecom wavelengths, Applied Physics Letters 82, no. 18, (5 May 2003) : 2954-6
22 Liu, Y.M. ; Xiao, X. ; Prucnal, P.R. ; Sturm, J.C. , All-optical switching in an asymmetric silicon Fabry-Perot etalon based on the free-carrier plasma effect, Applied Optics 33, no. 18, (20 June 1994) : 3871-4
23 Almeida, V. R., Barrios, C. A., Panepucci, R. R., Lipson, M., Foster, M.A., Quzounov, D. G., and A. L. Gaeta, "All-optical switching on a silicon chip", Optics Letters 29 (Dec. 2004)
24 Almeida, V. R., Barrios, C. A., Panepucci, R. R., Lipson, M., "All-Optical control of light on a Silicon chip", Nature, pp1081-1084 (Oct 2004)

PARTICIPANTS

The following personnel have participated and were funded by the project:

Principal investigator
Michal Lipson, Assistant professor, School of Electrical and computer Engineering, Cornell University

Postdoctoral associates
Sameer Pradhan, postdoctoral associate, School of Electrical and computer Engineering, Cornell University

Roberto Panepucci, postdoctoral associate, School of Electrical and computer Engineering, Cornell University

REFEREED PUBLICATIONS

1. Almeida, V. R., Barrios, C. A., Panepucci, R. R., Lipson, M., "All-Optical control of light on a Silicon chip", Nature, pp1081-1084 (Oct 2004)

Abstract

Photonic circuits in which beams of light redirect the flow of other beams of light, are a long-standing goal for developing highly integrated optical communication components. Ideally, circuits based on optical interconnects would be constructed using sub-micron-size devices in which photons are manipulated in a manner similar to the way electrons are manipulated in a semiconductor circuit. Furthermore, it is highly desirable to use silicon - the dominant material in the microelectronic industry - as the platform for these photonic chips. All-optical control of light on silicon is challenging due to its relatively weak non-linear optical properties. Here we present the first experimental demonstration of fast all-optical switching on silicon using highly light-confining structures to enhance the sensitivity of light to small changes in refractive index. The transmission of the structure can be modulated by up to 94% in less than 500 ps using light pulses with energies as low as 25 pJ. These results confirm the recent theoretical prediction by Barrios et al. of efficient optical switching in silicon using resonant structures1.

2. Almeida, V. R., Barrios, C. A., Panepucci, R. R., Lipson, M., Foster, M.A., Quzounov, D. G., and A. L. Gaeta, "All-optical switching on a silicon chip", Optics Letters 29 (Dec. 2004)

Abstract

We present an experimental demonstration of fast all-optical switching on a silicon photonic integrated device by employing a strong light-confinement structure to enhance sensitivity to small changes in the refractive index. By use of a control light pulse with

energy as low as 40 pJ, the optical transmission of the structure is modulated by more than 97% with a time response of 450 ps.

3. C. Angulo Barrios, V. R. Almeida, R. R. Panepucci, B. S. Schmidt, and M.Lipson, "Compact Silicon Tunable Fabry-Pérot Resonator With Low Power Consumption", IEEE Photonics Technology Letters, VOL 16, pp. 506, Nov. 2004

Abstract

We demonstrate a 20- m-long tunable optical resonator integrated on a silicon-on-insulator waveguide. The microresonator consists of a planar Fabry–Pérot microcavity defined by deep Si/SiO2 Bragg reflectors with a high finesse of 11.2. The device is electrically driven and shows a modulation depth as high as 53% for a power consumption of only 20 mW.

4. Barrios, C.A., Almeida, V. R., and M. Lipson, "Low-Power-Consumption Short-Length and High-Modulation-Depth Silicon Electro-Optic Modulator", IEEE Journal of Lightwave Technologies, Vol. 21, no.4, p.1089, April, 2003.

Abstract

In this paper, we propose and analyze a novel compact electro-optic modulator on a silicon-on-insulator (SOI) rib waveguide. The device confines both optical field and charge carriers in a micron-size region. The optical field is confined by using a planar Fabry-Perot microcavity with deep Si/SiO2 Bragg reflectors. Carriers are laterally confined in the cavity region by employing deep etched trenches. The refractive index of the cavity is varied by using the free-carrier dispersion effect produced by a p-i-n diode. The device has been designed and analyzed using electrical and optical simulations. Our calculations predict, for a 20-μm-long device, a modulation depth around 80% and a transmittance of 86% at an operating wavelength of 1.55 μm by using an electrical power under dc conditions on the order of 25 μW.

EXPENDITURES

Summary

The following table summarizes the cumulative expenditures of the project

Category	Period 8/1/02-7/31/03
Salaries	39,813.91
Fringe Benefits	9,849.98
Supplies	11,357.51
Travel	5,477.24
Equipment	2,223.99
Other	22,539.83
Total direct Cost	89,262.46
Indirect Cost	49,631.19
Total	138,893.19

Requisition

Miscellaneous laboratory tooling, supplies, computers and books

Travel

- Michal Lipson, CLEO, Baltimore, May 2003
- Vilson Almeida, CLEO, Baltimore, May 2003
- Roberto Panepucci, CLEO, Baltimore, May 2003
- Michal Lipson, Boston, MRS, Dec 2002

APPENDIX: PUBLISHED PAPERS

Low-Power-Consumption Short-Length and High-Modulation-Depth Silicon Electrooptic Modulator

Carlos Angulo Barrios, Vilson Rosa de Almeida, and Michal Lipson

Abstract—**In this paper, we propose and analyze a novel compact electrooptic modulator on a silicon-on-insulator (SOI) rib waveguide. The device confines both optical field and charge carriers in a micron-size region. The optical field is confined by using a planar Fabry–Pérot microcavity with deep Si/SiO_2 Bragg reflectors. Carriers are laterally confined in the cavity region by employing deep-etched trenches. The refractive index of the cavity is varied by using the free-carrier dispersion effect produced by a p-i-n diode. The device has been designed and analyzed using electrical and optical simulations. Our calculations predict, for a 20-μm-long device, a modulation depth of around 80% and a transmittance of 86% at an operating wavelength of 1.55 μm by using an electrical power under dc conditions on the order of 25 μW.**

Index Terms—**Bragg reflector, device modeling, Fabry–Pérot cavity, integrated optics, optical modulator, plasma dispersion effect, silicon optoelectronics.**

I. Introduction

SILICON-BASED photonic components working at 1.3- and 1.55-μm fiber-optic communications wavelengths for fiber-to-home interconnects and local area networks (LANs) are a subject of intensive research because of the possibility of integrating optical elements and advanced electronics together on a silicon substrate using bipolar or complementary metal–oxide–semiconductor (CMOS) technology [1]. The resulting optoelectronic integrated circuit (OEIC) should exhibit a better performance than optical and electrical circuits do when considered separately and present a significantly lower cost than those based on III–V semiconductor materials.

Si passive structures, such as waveguides, couplers, and filters have been extensively studied [2]–[4]. Less work has been reported on Si active (or tunable) integrated devices, such as modulators and switches, despite their importance as a means of manipulating light beams for information processing (e.g., coding–decoding, routing, multiplexing, timing, logic operations, etc.) in integrated optic circuits. Some Si-based thermooptic [5], [6] and electrooptic [7]–[20] active devices have been demonstrated. In thermooptic devices, the refractive index of Si is modulated by varying the temperature, inducing a phase modulation which, in turn, is used to produce an intensity modulation at the output of the device. For Si, the thermal change of the real optical refractive index is large [5]. Nevertheless, the thermooptic effect is rather slow and can only be used at up to 1-MHz modulation frequencies [6]. For higher modulation frequencies, up to a few hundred megahertz, electrooptic devices are required.

Most of the proposed electrooptic devices exploit the free carrier dispersion effect [21] to change both the real refractive index and optical absorption coefficient. This is because the unstrained pure crystalline Si does not exhibit linear electrooptic (Pockels) effect, and the refractive-index changes due to the Franz–Keldysh effect and Kerr effect are very weak. In free-carrier absorption modulators (FCAM), changes in the optical absorption of the structure are directly transformed into an output intensity modulation [18]. Phase modulation in a specific region of optical devices, such as Mach–Zehnder modulators, total-internal-reflection (TIR)-based structures, cross switches, Y switches and Fabry–Pérot (F-P) resonators, is also used to modulate the output intensity [7]–[20].

Free-carrier concentration in electrooptic devices can be varied by injection, accumulation, depletion, or inversion of carriers. Si-based electrooptic modulators (EOMs) based on p-i-n diodes, metal–oxide–semiconductor field-effect transistors (MOSFETs) and bipolar-mode field-effect transistor (BMFET) structures have been proposed [7]–[20], [22], [23]. Table I shows a comparison of all-silicon electrooptic intensity modulators and switches reported in the literature. Most of the listed devices present some common features: they require long interaction distances and injection current densities higher than 1 kA/cm^2 in order to obtain a significant modulation depth. Long interaction lengths are undesirable in order to achieve high levels of integration and miniaturization for fabricating low-cost compact chips. High current densities may induce thermooptic effect due to heating of the structure and cause an opposite effect on the refractive-index change as that produced by free-carrier dispersion, reducing its effectiveness. There is therefore an urgent need, from the integration point of view, for structures that can be implemented in a micron-size region offering low current density, low power consumption, and high modulation depth.

Microcavities allow for the confinement and enhancement of the optical field in a very small region. The transmission of these structures near their resonance is highly sensitive to small index changes in the cavity, making microcavities adequate for intensity modulation applications in a short length [15]. In addition, since the refractive-index modulation can be confined to the cavity region, the electrical power to produce the desired phase change can be made very small.

Manuscript received September 6, 2002; revised December 18, 2002. This work was supported in part by the Alliance for Nanomedical Technologies, Air Force Office of Scientific Research, and in part by the Defense Advanced Research Project Agency under Contract No. F49620-02-1-0396.

The authors are with the School of Electrical and Computer Engineering, Cornell University, Ithaca, NY 14853 USA.

Digital Object Identifier 10.1109/JLT.2003.810090

TABLE I
SILICON ELECTROOPTIC ACTIVE DEVICES REPORTED IN THE LITERATURE (FCAM=FREE-CARRIER ABSORPTION MODULATOR; F-P=FABRY–PÉROT; TIR=TOTAL INTERNAL REFLECTION; ZGDC=ZERO GAP DIRECTIONAL COUPLER; M=AMPLITUDE MODULATION DEPTH; J=CURRENT DENSITY; t_s=SWITCHING TIME; V.D.= VERTICAL DEVICE; DEM/(D)=DEMONSTRATED; PROP/(P)=PROPOSED)

Year	Author	Electrical structure	Optical structure	M (%)	J (kA/cm^2)	Power (mW)	t_s (ns)	Length (μm)	Dem./ Prop.
1987	Lorenzo et al. [7]	p-i-n	Cross switch	50	1.26	-	-	2000	D
1989	Hemenway et al. [8]	p-i-n	Mach-Zehnder	30	100.0	-	18	v.d.	D
1991	Treyz et al. [9]	p-i-n	FCAM	75	3.0	-	50	500	D
1991	Treyz et al [10]	p-i-n	Mach-Zehnder	65	1.6	-	<50	500	D
1991	Xiao et al. [11]	p-i-n	F-P	10	6.0	-	25	v.d.	D
1994	Liu et al. [12]	p-i-n	Y-switch	>90	9.0	-	200	800	D
1994	Liu et al. [13]	p-i-n	TIR-switch	>90	12.5	-	100	200	D
1995	Zhao et al. [14]	p-i-n	Mach-Zehnder	98	-	-	200	816	D
1995	Liu et al. [15]	p-i-n	F-P	80	-	-	-	20.9	P
1996	Zhao et al .[16]	p-i-n	ZGDC	97.2	1.027	123.7	210	1103	D
1997	Cutolo et al. [17]	p-i-n	Bragg reflector	50	-	4	24.7	3200	P
1997	Cutolo et al. [18]	BMFET	FCAM	20	2.3	126	6	1000	P
1997	Zhao et al. [19]	p-i-n	TIR	>88	8.8	-	110	190	D
2001	Coppola et al. [20]	p-i-n	Bragg reflector	94	-	0.3	5	3200	P

Carrier confinement in the active region of the electrooptic device is important in order to optimize the device performance. For example, the use of lateral trench isolation in a silicon p-i-n phase modulator has been predicted to improve both the dc and transient device performances [24]. This is because the lateral carrier diffusion that does not contribute to altering the refractive index in the central active region of the modulator is reduced, allowing a better use of the injected carriers. In addition, carrier confinement permits high-scale integration due to electrical isolation between neighbor devices.

We propose the use of the aforementioned advantages of microcavities (optical field confinement) and trench isolation (carrier confinement) in a planar silicon F-P cavity formed by high-index-contrast Si/SiO_2 distributed Bragg reflectors (DBRs) to design a compact low-drive-power and high-modulation-depth EOM in a silicon-on-insulator (SOI) ridge waveguide. The SOI ridge waveguide allows implementing a lateral p-i-n diode in the microcavity, and may exhibit optical losses less than 1.0 dB/cm at 1.55-μm wavelength [25].

This paper has been divided into the following sections. Section II describes the device structure. In Section III, the electrical and optical models used for the calculations are presented. In Section IV, results from the simulations are shown and discussed. This section is divided into electrical and optical characteristics. The electrical analysis includes dc and transient performance of the p-i-n/cavity configuration. The optical analysis comprises both the optical mode characteristics and the transmission properties of the device. Finally, a summary and conclusions are given in Section V.

II. DEVICE STRUCTURE

Fig. 1(a) and (b) shows a perspective and longitudinal-section schematics, respectively, of the EOM. For illustration purposes, the trenches down to the buried oxide (BOX) layer are drawn as empty in Fig. 1(a). In our simulations, these are assumed to be completely filled with SiO_2. The device consists of an F-P cavity formed by two DBRs in an SOI rib waveguide. The top silicon layer (device layer) is 1.5-μm-high (h_d) with an n-type background doping concentration of 10^{15} cm^{-3}. Both DBRs consist of the same number of Si/SiO_2 periods down to the BOX layer. The length of the Si and SiO_2 regions is denoted as L_{Si} and L_{ox}, respectively. Fig. 2 shows a schematic diagram of the cavity region. As in Fig. 1(a), the trenches are drawn as unfilled for better visualization. The rib width and height are chosen to be $w_{rib} = 1.5$ μm and $h_{rib} = 0.45$ μm, respectively. Two lateral trenches down to the BOX layer are assumed to be on both sides of the rib with a width of $w_{tr} = 150$ nm. The width of the cavity region delimited by the lateral trenches is W_{pin}. Heavily doped p^+ and n^+ regions are defined in the cavity region, at both sides of the rib, separated $w_{sep} = 0.5$ μm from the corresponding rib edge and extended to the corresponding lateral trench. A Gaussian doping profile is assumed for both highly doped regions with a maximum peak concentration of 10^{20} cm^{-3} at $y = [(h_d - h_{rib}) - 0.01\ \mu m] = 1.04$ μm, located along a line from $x = (W_{pin}/2)$ to $x = [(w_{rib}/2) + w_{sep}]$ for one doped region and from $x = -(W_{pin}/2)$ to $x = -[(w_{rib}/2) + w_{sep}]$ for the other one, and a standard deviation along the y axis of 0.05 μm. At $x > -[(w_{rib}/2) + w_{sep}]$ for one doped region and $x < [(w_{rib}/2) + w_{sep}]$ for the other one, the doping drops off laterally (along the x axis) with a standard deviation of 0.035 μm. The length of the highly doped regions is equal to that of the cavity (L_{cav}). Metal electrodes contact both the p^+ (anode) and n^+ (cathode) regions with the same width and length as those. A planar silicon dioxide layer covering the whole structure has been assumed.

III. DEVICE MODEL

The electrooptic device was electrically and optically modeled. An electrical model was used to study key parameters of the p-i-n/cavity that determine the device performance, such as

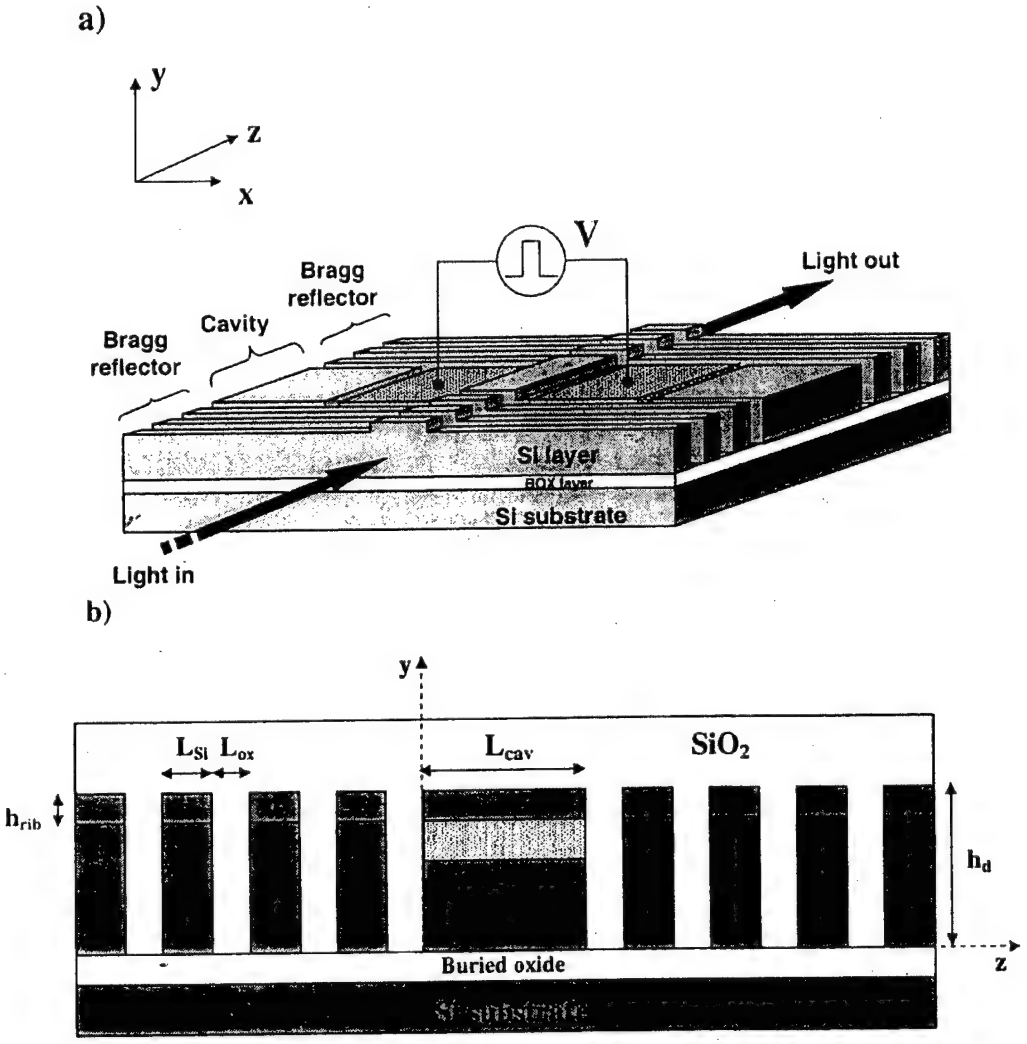

Fig. 1. (a) Silicon electrooptic modulator based on a p-i-n electrical structure in a Fabry–Pérot microcavity with high-reflectivity Bragg reflectors integrated in a single-mode SOI ridge waveguide. The output light is electrically controlled by a voltage generator (V). (b) Longitudinal cross section of the device.

free-carrier concentration and distribution in the cavity, injection current density, electrical power, and internal temperature under dc and transient conditions. An optical model was employed to design and analyze the Bragg reflectors and the cavity length in terms of transmission, modulation depth, and optical losses of the structure.

A. Electrical Model

A commercially available two-dimensional (2-D) and three-dimensional (3-D) simulation package, ATLAS from SILVACO [26], was employed to achieve the electrical calculations. The suitability of this device modeling software to analyze EOMs in SOI waveguides has been demonstrated by other authors [24], [27]. This program simulates internal physics and device characteristics of semiconductor devices by solving Poisson's equation and the charge continuity equations for electrons and holes numerically. The software allows a complete statistical approach (Fermi–Dirac statistics) when, for example, heavily doped regions are considered. Carrier recombination models include Shockley–Read–Hall (SRH) recombination, Auger recombination, and surface recombination. A concentration– and temperature-dependent model has been used to model the carrier mobility. The simulation package also includes thermal modeling, which accounts for Joule heating, heating and cooling due to carrier generation and recombination, and the Peltier and Thomson effects. The heat flow equation is solved for specific combinations of heat-sink structures, thermal impedances, and ambient temperatures.

In our simulations, a carrier concentration-dependent SRH recombination model has been employed, with an estimated carrier lifetime in the Si device layer (intrinsic region) of electrons and holes of $\tau_n = 700$ ns and $\tau_p = 300$ ns, respectively, for an n-type doping concentration of 10^{15} cm^{-3} [18].

Ohmic contacts without additional contact resistance or capacitance have been assumed. In addition, the electrical contacts (electrodes) were considered to act as thermal contacts (heat sinks) at a fixed temperature of 300 K.

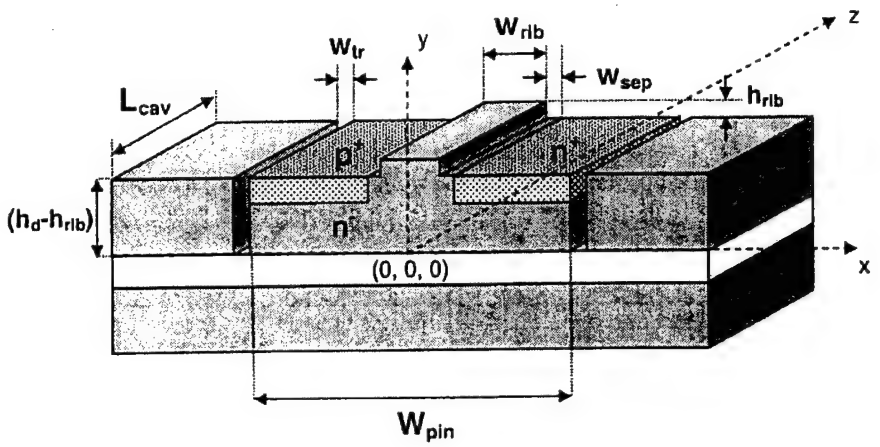

Fig. 2. Schematic of the microcavity. A lateral p-i-n diode is formed by defining two highly doped n and p regions at each side of the ridge, respectively. Two lateral trenches avoid carrier diffusion away from the cavity region.

B. Optical Model

We used the finite-difference time-domain (FDTD) method [28] and transfer matrix method (TMM) [29] for the optical analysis of the DBRs and F-P cavity. From the values of the electron and hole concentrations at any point of the p-i-n/cavity region, the induced real refractive index and optical absorption coefficient variations (Δn and $\Delta\alpha$, respectively) at a wavelength of 1.55 μm produced by free-carrier dispersion (highly doped regions and carrier injection in the cavity) are calculated by using [30]

$$\Delta n = \Delta n_e + \Delta n_h = -\left[8.8 \times 10^{-22} \cdot \Delta N + 8.5 \times 10^{-18} \cdot (\Delta P)^{0.8}\right] \quad (1)$$

$$\Delta\alpha = \Delta\alpha_e + \Delta\alpha_h = 8.5 \times 10^{-18} \cdot \Delta N + 6.0 \times 10^{-18} \cdot \Delta P \quad (2)$$

where

Δn_e	refractive-index change due to electron concentration change;
Δn_h	refractive-index change due to hole concentration change;
ΔN	electron concentration change in cm^{-3};
ΔP	hole concentration change in cm^{-3};
$\Delta\alpha_e(\text{in cm}^{-1})$	absorption coefficient variations due to ΔN;
$\Delta\alpha_h(\text{in cm}^{-1})$	absorption coefficient variation due to ΔP.

Diffraction losses and material optical absorption are calculated with the FDTD method. The fundamental mode of the waveguide is launched at the input and the reflected (R), and transmitted (T) powers are recorded by virtual detectors. Losses (A) are obtained by using the relation $R + T + A = 1$. Scattering losses, due to surface roughness, are neglected. We used a one-dimensional (1-D) model (along the propagation direction) based on the TMM to calculate the transmission and reflection spectra of the structure. The effect of the transverse and lateral geometry of the structure, the diffraction, and the absorption are considered in our 1-D model by using an equivalent complex effective refractive index obtained from the 3-D FDTD calculations of the entire structure for a short cavity length ($\lambda_p/2n_{\text{Si}}$, where $\lambda_p = 1.55$ μm and n_{Si} is the effective refractive index of the Si region). The purpose of using this technique is to simplify the calculations by employing a flexible model that allows predicting the optical performance of the device for different design parameters in a shorter time. Calculations obtained by using this FDTD-assisted TMM technique were in good agreement with those obtained by employing exclusively the FDTD method, which supports the suitability of our model.

IV. Results and Discussion

A. Electrical Analysis

1) DC Characteristics: We found that both electron (N) and hole (P) concentrations in the cavity region are nearly equal for forward-bias voltages between 0.8 and 1.1 V, assuming a surface recombination velocity of 10^2 cm/s at the interface between the Si cavity and the surrounding SiO_2. This surface recombination velocity may correspond to Si surfaces passivated with thermally grown SiO_2 [31]. The p-i-n diode operates under high injection condition within the considered forward-bias voltage range. As expected from previous works on larger structures [17], [27], the injected carrier distribution is highly uniform throughout the central region of the cavity. This result simplifies the optical calculations, since the spatial distribution of the refractive index and absorption coefficient in the cavity when carriers are injected in the guiding region can be considered uniform. A carrier concentration of $N = P = 3 \times 10^{17}$ cm^{-3} is predicted for a forward bias of 0.87 V, which induces a real refractive-index change of $\Delta n = -10^{-3}$ [see (1)] and an absorption coefficient variation of $\Delta\alpha = 4.35$ cm^{-1} [see (2)].

Our simulations show that some of the injected free carriers into the low-doped n-type Si layer spread laterally away from the central guiding region as the distance between the lateral trenches (W_{pin}) is increased, in agreement with previous works [24]. This leads to a leakage current component that increases the necessary dc power in order to obtain the targeted carrier concentration (refractive-index change) in the central guiding region. In particular, the dc power consumption for

TABLE II

TOTAL CURRENT DENSITY (J), PERCENTAGE OF THE CURRENT COMPONENT DUE TO SURFACE RECOMBINATION (J_s) TO THE TOTAL CURRENT (J), dc ELECTRICAL POWER (P_{dc}), AND FREE-CARRIER CONCENTRATION (N, P) IN THE CENTRAL REGION OF THE CAVITY FOR THREE SURFACE RECOMBINATION VELOCITIES AT THE Si/SiO_2 INTERFACES: (a) $S_p = S_n = 0$; (b) $S_p = S_n = 10^2$ cm/s; AND (c) $S_p = S_n = 10^5$ cm/s. A FORWARD-BIAS VOLTAGE OF 0.87 V AND A CAVITY LENGTH OF 1 μm ARE CONSIDERED

S_p, S_n (cm/s)	J (A/cm^2)	J_s/J (%)	P_{dc}(μW)	N, P (cm^{-3})
0	83.33	0	1.14	$3x10^{17}$
10^2	115.86	28.1	1.51	$3x10^{17}$
10^5	5514.6	98.5	71.9	$5x10^{16}$

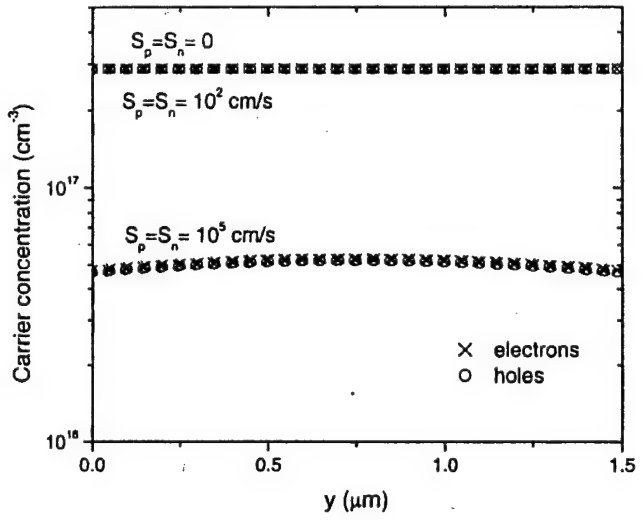

Fig. 3. Free-carrier distribution along the y axis at $x = 0$ μm and $z = L_{cav}/2$ for three different surface recombination velocities at the Si/SiO_2 cavity interface: (a) $S_p = S_n = 0$; (b) $S_p = S_n = 10^2$ cm/s; and (c) $S_p = S_n = 10^5$ cm/s. In all cases, a forward-bias voltage of 0.87 V is considered.

W_{pin} equal to 4.5, 8, and 12 μm was calculated to be 0.81, 1.51, and 2.27 μW per micrometer length, respectively, for a free-carrier concentration in the cavity of 3×10^{17} cm^{-3}. That is, the dc power increases 180% when W_{pin} is varied from 4.5 to 12 μm, indicating the need to confine carriers in the guiding region in order to reduce the drive dc power. Hereafter, we will assume a W_{pin} value of 8 μm as a compromise between low power consumption and good optical properties [see Section IV-B1)]. In the same way as occurs in the lateral direction (x axis), carriers may diffuse along the longitudinal direction (z axis) if no carrier confinement means are accounted. By using lateral and longitudinal trenches down to the BOX layer, electrical isolation of the cavity is achieved along all directions, leading to injection carrier confinement in the central guiding region, suppressing the leakage current due to carrier spreading.

Fig. 3 shows the electron and hole distribution along the y axis at $x = 0$ μm and $z = L_{cav}/2$ for a forward-bias voltage of 0.87 V and different surface recombination velocities (S_p and S_n, for holes and electrons, respectively). In case (a), no surface recombination ($S_p = S_n = 0$) is assumed; case (b) corresponds to thermally grown SiO_2 ($S_p = S_n = 10^2$ cm/s); and case (c) assumes no surface passivation ($S_p = S_n = 10^5$ cm/s). As expected, it is observed that for case (a), the carrier distribution is highly uniform. For case (b), the carrier distribution is not significantly affected with respect to case (a). On the other hand, for case (c), it is clear that the total carrier concentration has decreased with respect to the previous cases and does not present a uniform spatial distribution. Case (c) could correspond to a Si/SiO_2 interface in which SiO_2 has been placed by means other than thermal growth, such as, for example, chemical vapor deposition (CVD) or spin-on-glass (SOG) techniques.

Table II shows the drive current density (J), percentage of the current component due to surface recombination (J_s) to the total current (J), dc power (P_{dc}), and free-carrier concentration (N, P) in the central region of the cavity for the aforementioned surface recombination velocities. The current density is defined as the total injection current divided by the longitudinal cross-section area of the cavity at the middle ($x = 0$). In all the cases, a forward voltage of 0.87 V and a cavity length of 1 μm are assumed.

As expected, it is seen that the injection current and electrical power increase as the surface recombination velocity is increased. For case (b), the injection current component due to surface recombination (leakage current) represents 28.1% of the total current, whereas this leakage component reaches a significant 98.5% of the total injected current for case (c). The dissipated power for case (b) increases by 32.4%, as compared with case (a), as a consequence of leakage current via surface recombination; nevertheless, the total drive power is kept to a low value. These results indicate the importance of electrical passivation of the surfaces of the p-i-n/cavity region in order to reduce the component of the total current due to surface recombination and, therefore, the dc power consumption. In addition, surface passivation by thermal SiO_2 is also advantageous from the optical point of view, since it reduces the scattering losses from the surface [32]. Hereafter, a surface recombination velocity of $S_p = S_n = 10^2$ cm/s will be assumed. For this case, the calculated increase of the device temperature was less than 10^{-2} K.

It must be noted that the effect of the contact resistance of the electrodes on the total power is not significant for a forward injection current of 1.74 μA/μm (V = 0.87 V) if proper contact metallization is achieved. For example, if Co/Si contacts are assumed on both electrodes, the corresponding contact resistance values, after a rapid thermal annealing (RTA) process, on the highly doped n^+ and p^+ regions should be around 1.6×10^{-7} and 8.9×10^{-7} Ωcm^2, respectively [33]. This means a total series resistance due to the contacts of 38.2 Ω μm, which leads to a negligible increase of 1.1×10^{-10} W/μm in dc power consumption.

B. Transient Characteristics

We assumed an excitation voltage pulse with $V_{OFF} = 0$ V (OFF state) and $V_{ON} = 0.87$ V (ON state) for the transient analysis. The duration of both OFF and ON states is 300 ns,

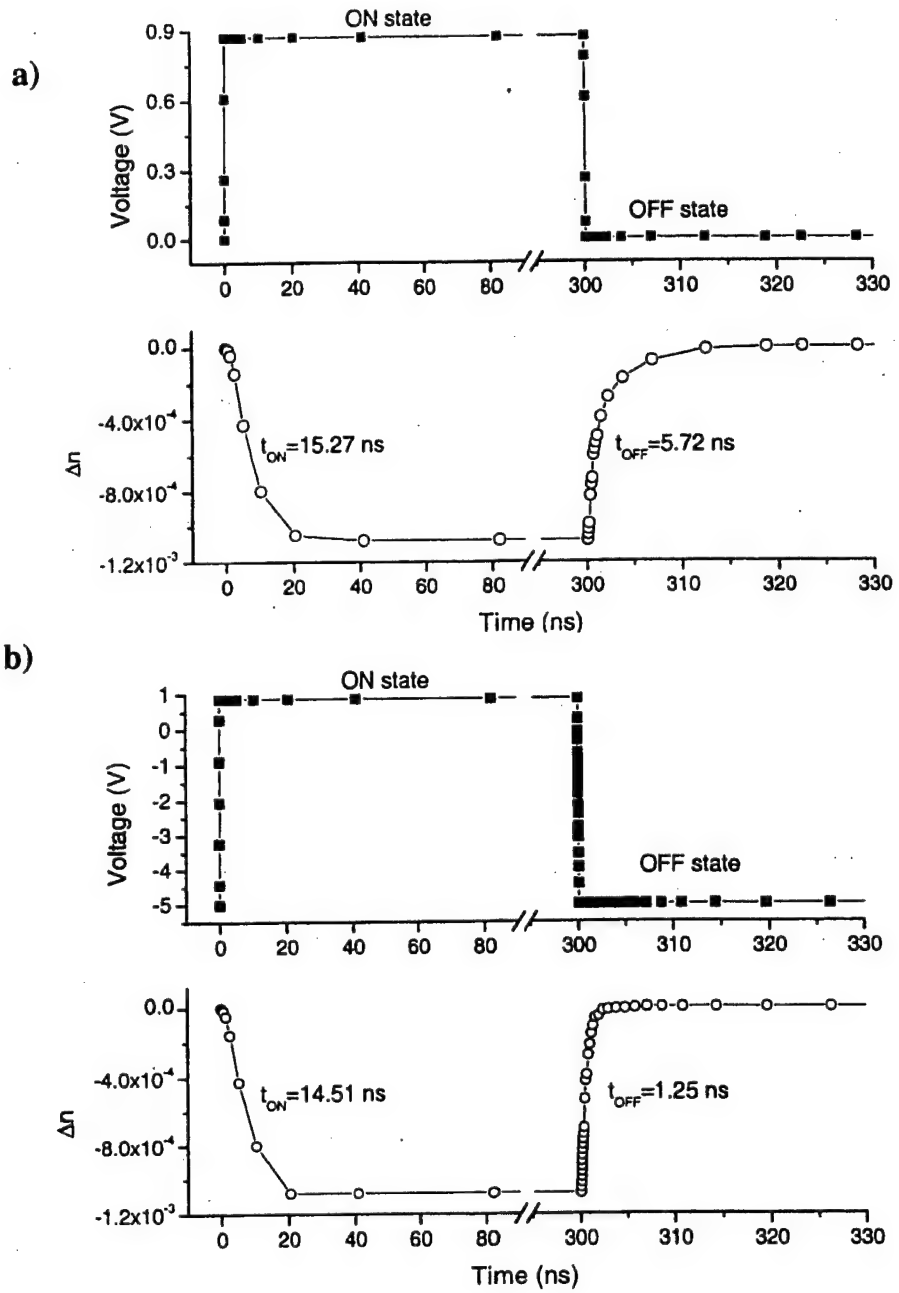

Fig. 4. (a) Transient behavior of the refractive-index change in the cavity (Δn) for a voltage pulse with $V_{ON} = 0.87$ V and $V_{OFF} = 0$ V. (b) Transient variation of Δn for $V_{ON} = 0.87$ V and $V_{OFF} = -5$ V. In both cases, the voltage pulse is 300 ns long for both ON and OFF states with ramp and fall times of 0.1 ns.

whereas both the rise time and fall time for the voltage bias step are 0.1 ns. Fig. 4(a) shows the excitation voltage pulse and the calculated refractive-index modulation (Δn) in the cavity due to free-carrier dispersion effect versus time. For the refractive-index modulation, we define the turn-on time (t_{ON}) as the time required for the refractive-index change (Δn) to change from 10% to 90% of its maximum absolute value ($|\Delta n|$). Likewise, the turn-off time (t_{OFF}) is defined as the time needed for the refractive-index change to vary from 90% to 10% of its maximum absolute value. It is seen that the turn-on time is longer than the turn-off time. The decrease of refractive index occurs because of carrier injection (forward bias) by diffusion from the highly doped regions into the intrinsic (low-doped) material. This is because the characteristic length for diffusive transport in the intrinsic region $l = (D_a \tau_{eff})^{1/2} = 5.2\ \mu$m [$D_a = 18$ cm^2/s is the ambipolar diffusion coefficient [9], and τ_{eff} ($= t_{ON} =$ 15.27 ns) is the effective carrier lifetime in the intrinsic region] is comparable to the lateral dimension of our device. On the other hand, the increase of refractive index results from depletion of carriers in the central guiding region. Carrier removal is achieved by both carrier recombination and the increased electric field across the intrinsic region. A higher reverse V_{OFF} would result in a shorter turn-off time, since the depletion electric field is increased. This is seen in Fig. 4(b) for

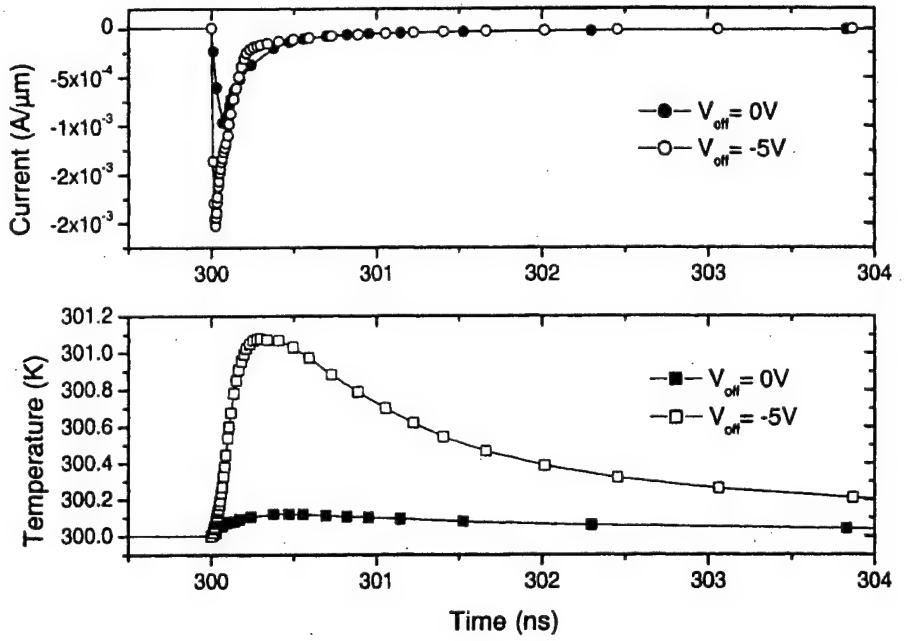

Fig. 5. Current and maximum device temperature transient response when the device is switched off from $V_{ON} = 0.87$ V to $V_{OFF} = 0$ V (filled circles and squares, respectively) and from $V_{ON} = 0.87$ V to $V_{OFF} = -5$ V (open circles and squares, respectively). The temperature of the thermal contacts (electrodes) is 300 K.

$V_{OFF} = -5$ V. The simulations reveal that both voltage rise and fall processes lead to the appearance of current peaks for a short time interval. In particular, a remarkable reverse current peak occurs during the transition from V_{ON} to V_{OFF}. Fig. 5 shows the transient current and maximum device temperature during the stepping down of the applied voltage from $V_{ON} = 0.87$ V to $V_{OFF} = 0$ V and -5 V. In both cases, it is observed that the transient reverse current peak (2×10^{-3} and 1×10^{-3} A/μm for $V_{OFF} = -5$ V and $V_{OFF} = 0$ V, respectively) is around three orders of magnitude higher than the corresponding steady-state current (1.74 μA/μm), and the maximum current for $V_{OFF} = -5$ V is twice higher than that reached for $V_{OFF} = 0$ V. The higher the reverse V_{OFF}, the shorter becomes the rise time and the larger the transient current peak. This leads to an appreciable increase of the device temperature, around 1 K for $V_{OFF} = -5$ V. For $\lambda = 1.55$ μm, the thermal change of refractive index of silicon is $\partial n/\partial T = +1.86 \times 10^{-4}$ K^{-1} [5]. That is, a maximum temperature increase of 1 K corresponds to an increase of the refractive index of $+1.86 \times 10^{-4}$, which is one order of magnitude smaller than that induced by the free-carrier dispersion ($\Delta n = -10^{-3}$). Therefore, the thermooptic effect for both $V_{OFF} = 0$ V and $V_{OFF} = -5$ V is predicted to be not significant.

Another factor that could limit the switching time of the device is the photon lifetime in the F-P cavity. The photon lifetime (τ_{ph}) corresponds to the time for the stored energy in the cavity to vanish after the external supply is shut off. However, the photon lifetime values for the considered device configurations [see Subsection IV-B2)] are calculated to be on the order of tens to hundreds of picoseconds, that is, much shorter than the switching times obtained in the electrical transient analysis. Therefore carrier diffusion, for the turn-on time, and carrier depletion, for the turn-off time, should be pointed out as the switching speed limiting factors in the device under study.

It must be noted that a larger value of W_{pin} would increase the switching time (t_s) since the refractive index must be changed (carrier injection and depletion) in a larger volume. For example, the calculated t_s for $W_{pin} = 12$ μm, $V_{ON} = 0.87$ V and $V_{OFF} = -5$ V is predicted to be 18.56 ns, that is, 17.7% larger than that calculated for $W_{pin} = 8$ μm.

C. Optical Analysis

1) Modal Characteristics: Our simulations show single-mode operation in the SOI rib waveguide for both transverse electric (TE) and transverse magnetic (TM) polarization modes, for $h_{rib} = 0.45$ μm, $w_{rib} = 1.5$ μm, and $h_d = 1.5$ μm. The distance between the lateral trenches $W_{pin} = 8$ μm was chosen in order to minimize the optical mode mismatch between the DBR and the cavity region, as well as the power consumption and switching time. Fig. 6 shows the intensity profile of the propagating fundamental TE mode (TE_{00}) for $W_{pin} = 8$ μm. The overlap integral between the TE_{00} mode in the cavity region and TE_{00} mode in the DBR region was calculated to be 99.99%. Lower W_{pin} values may lead to unstable single-mode operation. The free-carrier absorption losses of the propagating mode due to the highly doped p^+ and n^+ regions were found to be negligible because of the small overlap between these regions and the optical mode.

2) Transmission Characteristics: The lengths of the Si and SiO_2 regions of the DBRs were chosen according to the condition $n_{Si}L_{Si} + n_{ox}L_{ox} = \lambda_p/2$, where n_{Si} and n_{ox} are the effective refractive indexes of the Si and SiO_2 re-

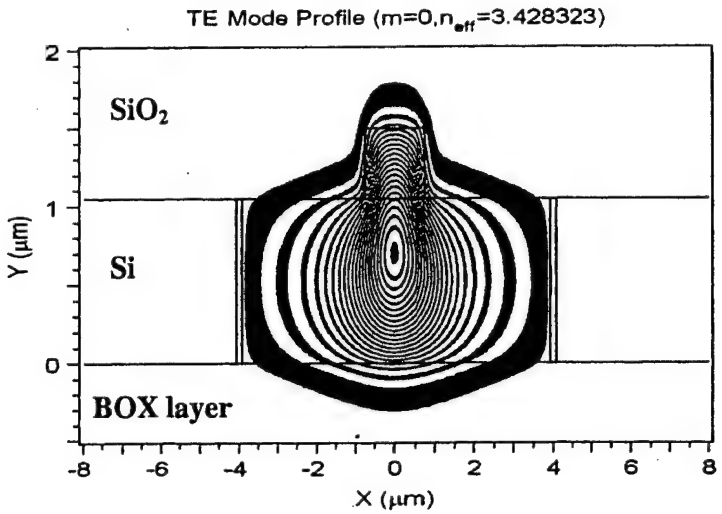

Fig. 6. TE_{00} mode distribution in the cavity for $W_{\text{pin}} = 8\ \mu\text{m}$, $h_{\text{rib}} = 0.45\ \mu\text{m}$, $w_{\text{rib}} = 1.5\ \mu\text{m}$, and $h_d = 1.5\ \mu\text{m}$.

gions, respectively, and $\lambda_p = 1.55\ \mu\text{m}$. In particular, we chose $L_{Si} = 160$ nm and $L_{ox} = 150$ nm, which lead to an optical path $n_{ox}L_{ox}$ smaller than $n_{Si}L_{Si}$ in order to minimize diffraction losses. The calculated reflectivity spectrum for the TE_{00} mode of a 6 Si/SiO_2-period DBR indicated a stopband of ~800 nm and a maximum reflectivity of 98.7% (transmittivity = 0.57% and diffraction losses = 0.73%).

The modulation depth (M) is defined as

$$M = 1 - \frac{T_{\text{MIN}}}{T_{\text{MAX}}} = \frac{P_{\text{OFF}} - P_{\text{ON}}}{P_{\text{OFF}}} \tag{3}$$

where $T_{\text{MAX(MIN)}}$ is the maximum(minimum) transmittivity, i.e., the ratio between the output in the OFF(ON) state and the input power P_{OFF} is the output optical power from the device when there is no free-carrier injection (OFF condition), and P_{ON} is the output optical power from the modulator when plasma injection occurs into the cavity (ON condition). Hereafter, the maximum transmittivity will be called just transmitivitty (T). The output optical power is calculated at $\lambda_p = 1.55\ \mu\text{m}$ (probe wavelength), which corresponds to a cavity resonance wavelength in the OFF condition. Table III shows the full-width at half-maximum (FWHM) of the spectral intensity ($\Delta\lambda$) of the resonance peak at 1.55 μm, modulation depth (M), transmittivity (T), and dc dissipated power (P_{dc}) for different cavity lengths and number of DBR periods. A refractive-index change in the cavity of $\Delta n = -10^{-3}$ is assumed. It is seen that 1) the modulation depth increases and 2) the transmittivity decreases as the number of periods is increased for a given cavity length. The first is due to the increase of the resonance peak sharpness (a decrease of $\Delta\lambda$) as a consequence of the increase of the DBR's reflectivity. The second is originated by the increase of the diffraction losses. The relation modulation depth -transmittivity is illustrated in Fig. 7, which shows the transmission characteristics of the device in the ON and OFF state for an $80(\lambda_p/2n_{Si})$-long cavity with three-period and four-period DBRs. Intensity attenuation due to the injected carriers in the ON state ($\alpha = 4.35\ \text{cm}^{-1}$) is observed. Although the use of a specific configuration may depend on the specific application, a good tradeoff between modulation depth (80%)

TABLE III
TRANSMISSION CHARACTERISTICS OF THE Si ELECTROOPTIC MODULATOR FOR A REFRACTIVE-INDEX CHANGE IN THE CAVITY $\Delta n = -10^{-3}$, TE_{00} OPTICAL MODE, $L_{Si} = 160$ nm, $L_{ox} = 150$ nm, AND PROBE WAVELENGTH $\lambda_p = 1.55\ \mu$m: FWHM OF THE RESONANCE PEAK ($\Delta\lambda$), MODULATION DEPTH (M), TRANSMITTIVITY (T), AND dc DISSIPATED POWER (P_{dc}) FOR VARIOUS CAVITY LENGTHS AND NUMBER OF PERIODS OF THE DBRs

L_{cav} (μm)	periods	Δλ (nm)	M (%)	T (%)	P_{dc} (μW)
5.684	3	1.275	27.6	86.3	7.8
$(25\lambda_p/2n_{Si})$	4	0.396	82.3	59.3	
	5	0.170	93.8	21.4	
9.074	3	0.807	50.3	86.3	12.3
$(40\lambda_p/2n_{Si})$	4	0.251	89.8	59.3	
	5	0.108	98.4	21.4	
18.117	3	0.408	80.8	86.3	24.5
$(80\lambda_p/2n_{Si})$	4	0.127	97.7	59.3	
	5	0.055	99.6	21.4	
22.638	3	0.327	86.8	86.3	30.6
$(100\lambda_p/2n_{Si})$	4	0.102	98.5	59.3	
	5	0.044	99.7	21.4	

and transmittivity (86%) is obtained for a $\sim 18 - \mu$m-long cavity with three-period DBRs, which represents a total device length of $\sim 20\ \mu$m. It must be noted the low values of the electrical power shown in Table III as well as the small refractive-index change in the cavity (0.1%) required to achieve high modulation depths.

The feasibility of producing high-aspect-ratio trenches on SOI with high verticality has been demonstrated by other authors [34], [35]. Nevertheless, deviations from the considered dimensions of the optical structure (length of the DBRs and cavity) due to fabrication tolerances may affect the predicted device performance. We estimated the effect of fabrication errors on the spectral transmittance by calculating the transmittivity spectra for different length deviations of the structure using the effective-index method together with the TMM, and calculating their average. Fig. 8 shows the calculated spectral transmittivity for the case considered in Fig. 7 (three-period DBR) for a maximum length deviation of 20 nm (that is, $L_{Si} = 160 \pm 10$ nm, $L_{ox} = 150 \pm 10$ nm, and $L_{cav} = 18.097 \pm 0.010\ \mu$m), 10 nm, and 5 nm. The length deviation of the DBR and cavity was assumed to be the same

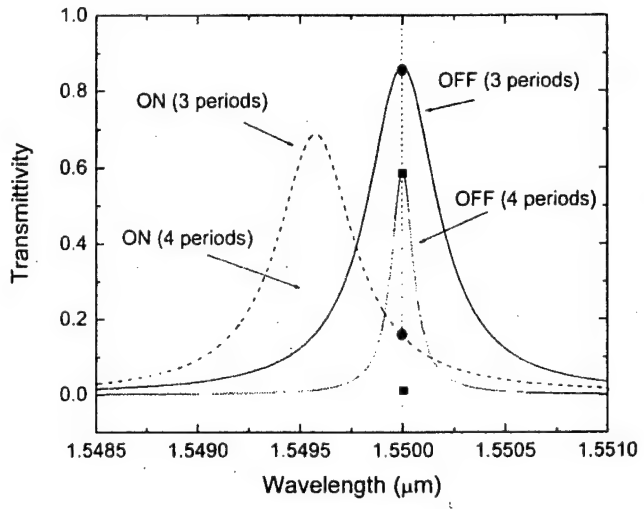

Fig. 7. Spectral transmittance for the TE_{00} optical mode of the simulated Si modulator in the OFF ($\Delta n = 0$) and ON ($\Delta n = -10^{-3}$) states for a three-period DBR device and a four-period DBR device. In both cases, the length of the cavity is $80(\lambda_p/2n_{Si}) = 18.1$ μm. The circles and squares illustrate the modulation depth at $\lambda_p = 1.55$ μm for the three-period and four-period device, respectively.

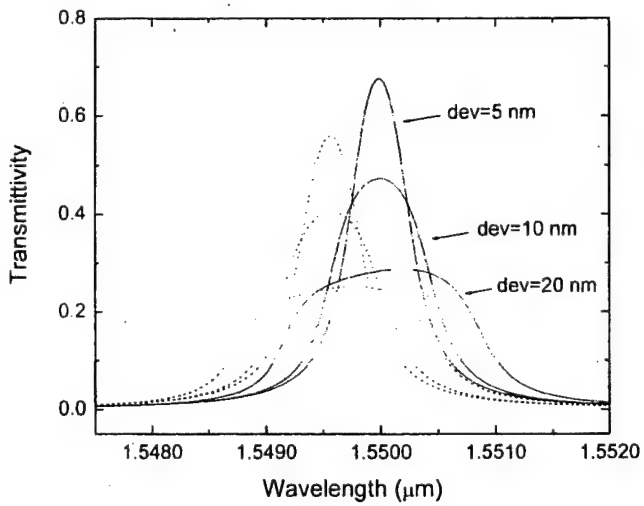

Fig. 8. Effect of length deviations of the DBR regions and cavity on the spectral transmittance with respect to the ideal case shown in Fig. 7 (three-period DBR). Maximum deviations (dev) of 20, 10, and 5 nm are considered. The OFF ($\Delta n = 0$) and ON ($\Delta n = -10^{-3}$) states are indicated by solid and dashed lines, respectively.

and the period of the DBR constant. It is seen that the resonance peak shape becomes degraded as the length deviation increases. This is mainly due to the variations of the cavity length, which shift the resonance wavelength for each length component, broadening the averaged resonance peak. As a consequence, the transmitivitty is considerably reduced as compared to the ideal case (see Fig. 7 for three-period DBR). It is also observed that high modulation depths can still be achieved (~72% at 1.5508-μm wavelength for a 20-nm-length deviation). Our simulations showed that if the considered length variations occur only in the DBR regions, the transmission spectrum is not significantly affected with respect to the ideal case.

V. Summary and Conclusion

We have analyzed the performance of a new planar silicon EOM based on an F-P microcavity by deep high-index-contrast Si/SiO_2 Bragg reflectors and confinement of free-carrier plasma dispersion in an SOI rib waveguide. Free-carrier concentration change in the cavity region produced by an integrated lateral p-i-n diode induces a refractive-index change that modulates the output power at a 1.55-μm wavelength. Deep lateral trenches in the p-i-n/cavity region laterally confine the injected carriers into the cavity. Deep Si/SiO_2 DBRs confine longitudinally 1) the free carriers and 2) the optical field into the cavity region. The device has been analyzed by using electrical and optical models.

Our analysis shows that a distance of $W_{pin} = 8$ μm between the cavity lateral trenches permits minimization of a) the dc electrical power and switching time of the device and b) the mode mismatch between the cavity and the DBRs. Electrical passivation of the cavity surfaces with thermal SiO_2 ($S_p = S_n = 10^2$ cm/s) is predicted to reduce the leakage current due to surface recombination by 70% as compared with a nonpassivated surface cavity ($S_p = S_n = 10^5$ cm/s), without significantly affecting the injection carrier concentration as compared with the case of no surface recombination ($S_p = S_n = 0$ cm/s). Diffraction is found to be the main cause of optical power losses in our device for $\Delta n = -10^{-3}$ in the cavity. Calculations show that a tradeoff between modulation depth and transmittivity of the device must be considered.

A 20-μm-long device with $S_p = S_n = 10^2$ cm/s, $W_{pin} = 8$ μm, and electrical contacts acting as heat sinks is predicted to exhibit ~80% of modulation depth with a transmittivity of ~86% at 1.55-μm operation wavelength by using ~ 25 μW of electrical power and a drive current density of 116 A/cm^2 under dc operation, leading to an increase of the device temperature $< 10^{-2}$K. The switching speed of this device is calculated to be ~16 ns for $V_{ON} = 0.87$ V and $V_{OFF} = -5$ V, with no significant thermooptic effect. To our knowledge, the estimated dc power consumption for this device is at least one order of magnitude smaller than the smallest reported (theoretical) value [20]. These characteristics reveal the benefits of confining both the optical field and the injection carriers in the cavity region in order to improve the EOM performance in terms of power consumption, current density, device length, and modulation depth. Si CMOS process compatibility makes this device very promising for low-cost and low-power silicon-based integrated photonic systems on a chip (PSOC) for low-frequency applications, such as LANs, fiber-to-home return links, interconnects, and sensor systems for chemical and biochemical applications.

Acknowledgment

The authors thank Dr. R. Panepucci and B. Schmidt for useful discussions.

References

[1] R. A. Soref, "Silicon-based optoelectronics," *Proc. IEEE*, vol. 81, pp. 1687–1706, Dec. 1993.

[2] U. Fischer, T. Zinke, J.-R. Kropp, F. Arndt, and K. Petermann, "0.1 dB/cm waveguide losses in single-mode SOI rib waveguides," *IEEE Photon. Technol. Lett.*, vol. 29, pp. 647–648, May 1996.

[3] P. Trinh, S. Yegnanaray, and B. Jalali, "5 × 9 integrated optical start coupler in silicon-on-insulator," *IEEE Photon. Technol. Lett.*, vol. 8, pp. 794–796, 1996.
[4] T. W. Ang, G. T. Reed, A. Vonsovici, A. G. Evans, P. R. Routley, and M. R. Josey, "Effects of grating heights on highly efficient unibond SOI waveguide grating couplers," *IEEE Photon. Technol. Lett.*, vol. 12, pp. 59–61, Jan. 2000.
[5] G. Cocorullo and I. Rendina, "Thermo-optical modulator at 1.5 μm in silicon etalon," *Electron. Lett.*, vol. 28, no. 1, p. 83, 1992.
[6] C. Cocorullo, M. Iodice, I. Rendina, and P. M. Sarro, "Silicon thermo-optical micro-modulator with 700 kHz −3 dB bandwidth," *IEEE Photon. Technol. Lett.*, vol. 7, pp. 363–365, Apr. 1995.
[7] J. P. Lorenzo and R. A. Soref, "1.3 μm electro-optic silicon switch," *Appl. Phys. Lett.*, vol. 51, no. 1, p. 6, 1987.
[8] B. R. Hemenway, O. Solgaard, and D. M. Bloom, "All-silicon integrated optical modulator for 1.3 μm fiber-optic interconnects," *Appl. Phys. Lett.*, vol. 55, no. 4, p. 349, 1989.
[9] G. V. Treyz, P. G. May, and J.-M. Halbout, "Silicon optical modulators at 1.3 μm based on free-carrier absorption," *IEEE Electron Device Lett.*, vol. 12, p. 276, June 1991.
[10] ——, "Silicon Mach–Zehnder waveguide interferometers based on the plasma dispersion effect," *Appl. Phys. Lett.*, vol. 59, no. 7, p. 771, 1991.
[11] X. Xiao, J. C. Sturm, K. K. Goel, and P. V. Schwartz, "Fabry–Pérot optical intensity modulator at 1.3 μm in silicon," *IEEE Photon. Technol. Lett.*, vol. 3, p. 230, Mar. 1991.
[12] Y. L. Liu, E. K. Liu, S. L. Zhang, G. Z. Li, and J. S. Luo, "Silicon 1 × 2 digital optical switch using plasma dispersion," *Electron. Lett.*, vol. 30, no. 2, p. 130, 1994.
[13] Y. Liu, E. Liu, G. Li, S. Zhang, J. Luo, F. Zhou, M. Cheng, B. Li, and H. Ge, "Novel silicon waveguide switch based on total internal reflection," *Appl. Phys. Lett.*, vol. 64, no. 16, p. 2079, 1994.
[14] C. Z. Zhao, G. Z. Li, E. K. Liu, Y. Gao, and X. D. Liu, "Silicon on insulator Mach–Zehnder waveguide interferometers operating at 1.3 μm," *Appl. Phys. Lett.*, vol. 67, no. 17, p. 2448, 1995.
[15] M. Y. Liu and S. Chou, "High-modulation-depth and short-cavity-length silicon Fabry–Pérot modulator with two grating Bragg reflectors," *Appl. Phys. Lett.*, vol. 68, no. 2, p. 170, 1995.
[16] C. Z. Zhao, E. K. Liu, G. Z. Li, Y. Gao, and C. S. Guo, "Zero-gap directional coupler switch integrated into a silicon-on-insulator for 1.3-μm operation," *Opt. Lett.*, vol. 21, no. 20, p. 1664, 1996.
[17] A. Cutolo, M. Iodice, A. Irace, P. Spirito, and L. Zeni, "An electrically controlled Bragg reflector integrated in a rib silicon on insulator waveguide," *Appl. Phys. Lett.*, vol. 71, no. 2, p. 199, 1997.
[18] A. Cutolo, M. Iodice, P. Spirito, and L. Zeni, "Silicon electro-optic modulator based on a three terminal device integrated in a low-loss single-mode SOI waveguide," *J. Lightwave Technol.*, vol. 15, p. 505, Mar. 1997.
[19] C. Z. Zhao, A. H. Chen, E. K. Liu, and G. Z. Li, "Silicon-on-insulator asymmetric optical switch based on total internal reflection," *IEEE Photon. Technol. Lett.*, vol. 9, p. 1113, Aug. 1997.
[20] G. Coppola, A. Irace, M. Iodice, and A. Cutolo, "Simulation and analysis of a high-efficiency silicon optoelectronic modulator based on a Bragg mirror," *Opt. Eng.*, vol. 40, no. 6, pp. 1076–1081, 2001.
[21] R. A. Soref and B. R. Bennett, "Electrooptical effects in silicon," *IEEE J. Quantum Electron.*, vol. 23, p. 123, Jan. 1987.
[22] S. R. Giguere, L. Friedman, R. A. Soref, and J. P. Lorenzo, "Simulation studies of silicon electro-optic waveguides devices," *J. Appl. Phys.*, vol. 68, no. 10, p. 4964, 1990.
[23] G. Breglio, A. Cutolo, A. Irace, P. Spirito, L. Zeni, M. Iodice, and P. M. Sarro, "Two silicon optical modulators realizable with a fully compatible bipolar process," *IEEE J. Select. Topics Quantum Electron.*, vol. 4, p. 1003, Nov./Dec. 1998.
[24] P. D. Hewitt and G. T. Reed, "Improved modulation performance of a silicon p-i-n device by trench isolation," *J. Lightwave Technol.*, vol. 19, p. 387, Mar. 2001.
[25] J. Schmidtchen, A. Splett, B. Schuppert, K. Petermann, and G. Burbach, "Low-loss singlemode optical waveguides with large cross section in silicon-on-insulator," *Electron. Lett.*, vol. 27, pp. 1486–1488, 1991.
[26] SILVACO Int., , Santa Clara, CA.
[27] P. D. Hewitt and G. T. Reed, "Improving the response of optical phase modulators in SOI by computer simulation," *J. Lightwave Technol.*, vol. 18, p. 443, Mar. 2000.
[28] [Online]. Available http://www.rsoftinc.com/fullwave.htm
[29] S. G. Lipson, H. Lipson, and D. S. Tannhauser, *Optical Physics*, 3rd ed. Cambridge, U.K.: Cambridge Univ. Press, 1995.
[30] R. A. Soref and B. R. Bennett, "Kramers–Kronig analysis of E-O switching in silicon," *SPIE Integr. Opt. Circuit Eng.*, vol. 704, 1986.
[31] D. R. Lim, "Device integration for silicon microphotonic platforms," Ph.D. dissertation, Mass. Inst. Technol., Cambridge, 2000.
[32] K. K. Lee, D. R. Lim, and L. C. Kimerling, "Fabrication of ultralow-loss Si/SiO_2 waveguides by roughness reduction," *Opt. Lett.*, vol. 26, no. 23, pp. 1888–1890, 2001.
[33] O. Nakatsuka, T. Ashizawa, H. Iwano, S. Zaima, and Y. Yasuda, "Contact resistivities and electrical characteristics of Co/Si contact by rapid thermal annealing," in *Proc. Advanced Metallization Conf. 1998 (AMC 1998)*, vol. 784, Warrendale, PA, 1999, pp. 605–610.
[34] M. Naydenkov and B. Jalali, "Fabrication of high aspect ratio photonic bandgap structures on silicon-on-insulator," *Proc. SPIE*, vol. 3936, pp. 33–39, 2000.
[35] M. Wasilik and A. P. Pisano, "Low frequency process for silicon on insulator deep reactive ion etching," *Proc. SPIE*, vol. 4592, pp. 462–472, 2001.

Carlos Angulo Barrios received the degree of Telecommunications Engineer from the Universidad Politécnica de Madrid (UPM), Madrid, Spain, in 1998, and the Ph.D. degree from the Royal Institute of Technology (KTH), Stockholm, Sweden, in 2002. His dissertation focused on the fabrication, performance, and analysis of GaAs-based buried-heterostructure lasers with Al-free semi-insulating materials regrowth.

In May 2002, he joined the Nanophotonics Group at the School of Electrical and Computer Engineering, Cornell University, Ithaca, NY, as a Postdoctoral Fellow. His work includes design, fabrication, and characterization of integrated photonic devices.

Vilson Rosa de Almeida was born in Brazil. He received the B.S. (*magna cum laude*) and M.S. degrees, both in electrical engineering, from Instituto Tecnologico de Aeronautica (ITA), Sao Jose dos Campos, Brazil, in 1997 and 1998, respectively. He is currently working toward the Ph.D. degree in electrical engineering with Cornell University, Ithaca, NY.

From 1998 to 2000, he conducted research on optical fiber sensors at Instituto de Estudos Avancados (IEAv-CTA), Sao Jose dos Campos, Brazil. His research interest areas are nanophotonic devices, optical fiber sensors, and photonic crystals.

Michal Lipson received the Ph.D. degree in semiconductor microcavities from The Technion—Israel Institute of Technology, Haifa, in 1999.

Subsequently, she was a Postdoctoral Associate in the Department of Material Science, Massachusetts Insitute of Technology (MIT), Cambridge. Her research at MIT was concerned with the physics and applications of Si-based photonic structures for on-chip applications. In July 2001, she joined the School of Electrical and Computer Engineering, Cornell University, Ithaca, NY, where she is an Assistant Professor studying nanophotonic structures.

Compact Silicon Tunable Fabry–Pérot Resonator With Low Power Consumption

C. Angulo Barrios, V. R. Almeida, *Student Member, IEEE*, R. R. Panepucci, B. S. Schmidt, and M. Lipson, *Member, IEEE*

***Abstract*—We demonstrate a 20-μm-long tunable optical resonator integrated on a silicon-on-insulator waveguide. The microresonator consists of a planar Fabry–Pérot microcavity defined by deep Si/SiO_2 Bragg reflectors with a high finesse of 11.2. The device is electrically driven and shows a modulation depth as high as 53% for a power consumption of only 20 mW.**

***Index Terms*—Bragg reflector, Fabry–Pérot (F-P) cavity, integrated optics, optical modulator, silicon optoelectronics.**

I. Introduction

SILICON-BASED optical tunable (or active) devices, such as modulators, switches, and variable attenuators working at 1.3 and 1.55-μm fiber-optic communications-wavelengths are key components for the realization of Si CMOS optoelectronic circuits for applications such as fiber-to-home and local area networks [1]. Since crystalline Si does not exhibit linear electro-optic (Pockels) effect, Si active devices use either the thermooptic effect [2] or the free-carrier plasma dispersion effect to change the refractive index of Si and to produce a phase modulation. Typical changes of the refractive index due to these effects are small (on the order of 10^{-3}). Therefore, optical structures such as Mach–Zehnder interferometers [3], directional couplers [4], and low finesse Fabry–Pérott (F-P) cavities [2], [5], which transform the phase modulation into an intensity modulation, require long interaction lengths and high power consumption in order to achieve significant modulation depths. These long lengths and high powers are undesirable in order to achieve high levels of integration.

High finesse microcavities are very attractive for implementing active optical devices in a short length since the transmission close to their resonance wavelengths is highly sensitive to small index changes in the cavity [6]. In addition, since the refractive index variation may be achieved only in the microcavity region, the modulating power (for either heating or changing the free carrier concentration) required to produce the desired phase change can be made very small.

In this letter, we report on the fabrication and characterization of a 20-μm-long tunable F-P cavity on silicon-on-insulator (SOI). The F-P microcavity is defined on a rib waveguide by deep etched Si/SiO_2 distributed Bragg reflectors (DBRs). The use of deep DBRs increases significantly the reflectivity of the mirrors as compared with previous works [2], [5] and, therefore, the finesse of the cavity. The discussed structure is based on a p-i-n junction. As we showed theoretically in [6], such a configuration is expected to exhibit a very high modulation depth due to the electro-optic (plasma dispersion) effect. Here, we show experimentally that surface recombination induces a thermal modulation mechanism that dominates over the electro-optic effect. Most of the previously reported modulators based on the thermooptic effect are usually rather slow and/or require significant power consumption [2]. In this work, however, we demonstrate that due to the high finesse of the F-P cavity, significant modulation depth can be achieved using a drive power as low as 20 mW.

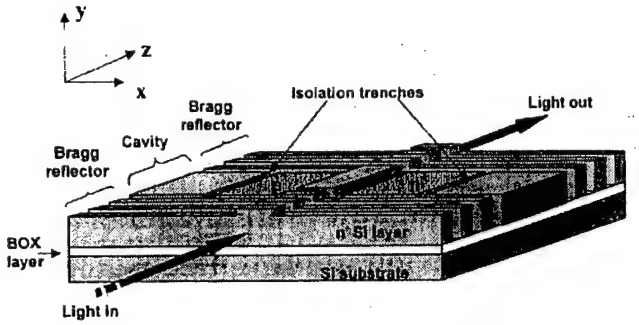

Fig. 1. Planar tunable F-P microcavity with deep Bragg reflectors and a p-i-n diode integrated on a single-mode SOI rib waveguide.

II. Device Structure and Fabrication

Fig. 1 shows a schematic of the device [6]. It was fabricatdon an SOI wafer with a 1.5-μm-thick undoped Si layer and a 1-μm-thick buried oxide (BOX) layer. DBRs and isolation trenches were patterned by electron-beam (EB) lithography and etched by Cl_2 -based reactive ion etching (RIE) down to the BOX layer using SiO_2 as a mask. The DBR period and length of the trenches were ~311 nm and ~173 nm, respectively. SiO_2 was thermally grown to passivate the etched Si surfaces. The trenches were filled with SiO_2 by using low-pressure chemical vapor deposition. The rib waveguide was defined by photolithography and etched by CF_4-based RIE using photoresist as a mask. The height and width of the rib were ~0.43 μm and ~1 μm, respectively. SiO_2 was thermally grown for surface passivation of the rib sidewalls. Then, a 1-μm-thick SiO_2 cladding layer was deposited by plasma-enhanced chemical vapor deposition. Rectangular openings in the SiO_2 cladding layer were

Manuscript received July 30, 2003; revised October 8, 2003. This work was supported by the National Science Foundation under Contract ECS-0300387 and the Defense Advanced Research Project Agency under Contract F49620-02-1-0396

The authors are with the School of Electrical and Computer Engineering, Cornell University, Ithaca, NY 14853 USA (e-mail: cb265@cornell.edu).

Digital Object Identifier 10.1109/LPT.2003.822251

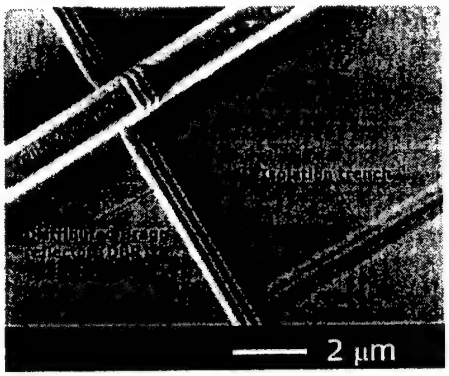

Fig. 2. Top view SEM photograph of a DBR and an isolation trench of the fabricated device.

made by EB lithography and CHF_3-based RIE for defining the doped regions shown in Fig. 1. Shallow n^+ and p^+ regions were created by ion implantation of As and BF_2, respectively. Ti and Al were deposited to form ohmic contacts and contact pads, respectively. Finally, the chip was cleaved, and the input and output facets were mechanically polished. Fig. 2 shows a scanning electron microscope (SEM) photograph of the planar F-P microcavity before doping.

III. Results and Discussion

Transmission experiments were performed by using a tunable laser (1520–1620 nm) as the input optical source. The probe beam was coupled directly into the rib waveguides by using a tapered-lensed fiber, collected by an output lens, and recorded by a photodetector. All the transmission experiments were made under transverse electric (TE) polarization. For the sake of normalization and waveguide loss evaluation, the transmitted power of a waveguide without any device was also measured.

Waveguide losses were evaluated by employing the F-P technique. Assuming a reflectivity of 0.3 at the Si/air interfaces, the measured losses in the rib waveguide for the TE-like polarized light were 22 dB/cm at $\sim$1.553 μm wavelength. We attribute this to scattering losses due to surface roughness of the rib sidewalls produced by the etching that, as indicated in [7], are significant for small rib widths. The coupling efficiency between the waveguide and the tapered-lensed fiber was measured to be around 8%. A theoretical coupling efficiency (integral overlap between the waveguide and fiber modes) of 20% was calculated by the beam propagation method (BPM). The discrepancy between the experimental and theoretical values may arise from facet polishing imperfections and fiber-waveguide alignment deviations. A fiber-to-waveguide tapered coupler similar to that reported in could be used to improve the coupling efficiency.

Fig. 3 (solid line) shows the transmission spectrum of the fabricated microcavity over the 1520–1600-nm wavelength range. The full width at half maximum (FWHM) of the resonance peak at $\lambda_p \sim 1.553$ μm is 1.54 nm. This represents a finesse, which is defined as the ratio between the full spectral range and the FWHM, of 11.2. A theoretical curve obtained by using a model described in [6] is also shown in Fig. 3 (dashed line). In

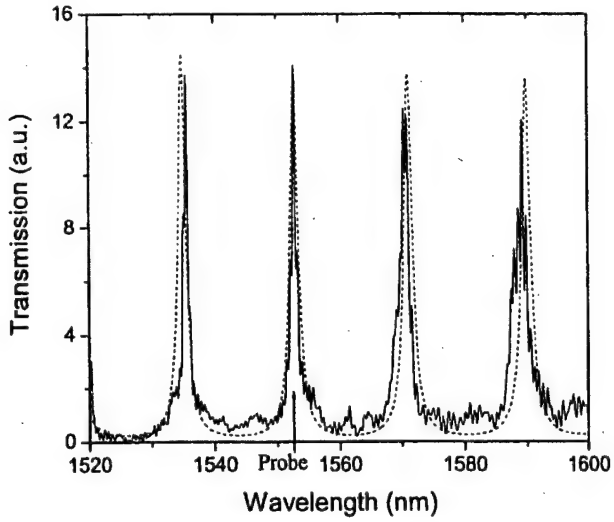

Fig. 3. Experimental (solid line) and calculated (dashed line) transmission spectra of the F-P microcavity for the fundamental TE-like mode in the 1520–1600-nm wavelength range.

this model, we include the experimental cavity internal loss of 0.04 dB [22 dB/cm (waveguide loss) $\times$ 18.12×10^{-4} cm (cavity length)]. A fitting parameter that models the scattering losses in the DBRs was introduced. From comparison with the experimental spectrum, we estimate the scattering losses in the DBRs to be 7 dB. These are much higher than those in the waveguide due to the larger area of the etched surfaces that form the DBRs. One can see good fit around the considered resonance peak λ_p between the experimental and calculated curves. If the cavity internal losses are neglected and the DBRs are assumed to be scattering lossless, the theoretical analysis revealed FWHM and finesse values of 0.33 nm and 57.3, respectively.

The transient optical characteristics of the fabricated device were studied by applying an electrical pulse of 100 Hz and a 50% duty cycle. We measured rise and fall times of 1.05 and 1.19 ms, respectively, of the output optical power at $\lambda =$ 1552.89 nm and a drive current pulse (I) of 5.4 mA. A red-shift of the transmission spectrum of the biased device was also observed. This is a known signature of a thermooptic effect in Si (positive thermooptic coefficient [2]). We did not observe any effect on the output optical signal that could be attributed to dominating free carrier plasma dispersion. This may be due to the high sensitivity of the device to surface passivation [6]. High surface recombination may reduce significantly the total carrier lifetime, increasing the needed drive current to inject a significant amount of carriers. Thus, by increasing the current, the power dissipated in the series resistance of the p-i-n is increased, resulting in the heating of the cavity and leading to the strong thermooptic modulation effect. An improved surface passivation should enable modulation due to free-carrier dispersion effect [6]. The transient response exhibited by our device make it suitable to be used as a variable optical attenuator or as a modulator for low-frequency applications such as home and consumer appliances and remote environmental sensors.

Fig. 4 (squares) shows the measured modulation depth (M) of the device at a probe wavelength (λ_{pb}) of 1552.89 nm as a function of the dissipated power (P_d). M is defined as (P_{OFF} –

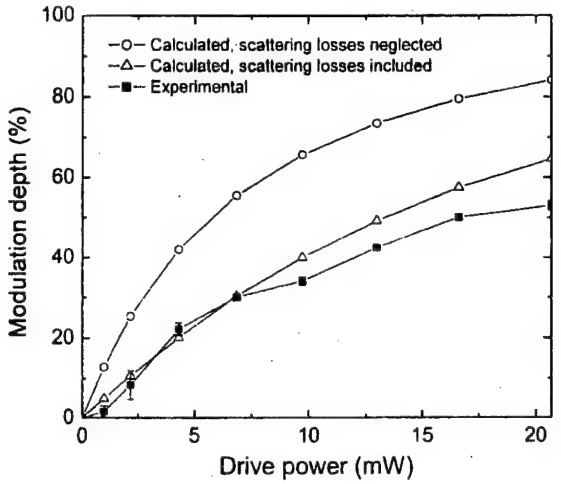

Fig. 4. Experimental (square dots) and calculated (triangular dots) modulation depth of the studied device at $\lambda_{pb} = 1552.89$ nm as a function of the dissipated power. The calculated modulation depth of a similar device with negligible scattering losses is shown in circular dots.

$P_{ON})/P_{OFF}$, where P_{OFF} and P_{ON} are the transmitted optical powers in the OFF ($I = 0$) and ON ($I \neq 0$) states, respectively. A maximum modulation depth of 53% is obtained at $P_d = 20$ mW ($I = 5.4$ mA). This dissipated power is two orders of magnitude smaller than that reported for longer F-P cavity devices for a similar modulation depth [2], [5]. The small value of the power consumption should be attributed to the small size and high finesse of our F-P microcavity.

The dependence of the change in index with temperature $\Delta n_{eff}/\Delta T$ provides an indication of the relative contributions of the free-carrier effect and the thermal effect to the modulation of the signal. This dependence can be estimated from a) the change in effective index as a function of the dissipated power and b) the temperature change for a given drive power. a) The change in effective index as a function of the dissipated power is obtained from the wavelength shift ($\Delta\lambda$) for a given modulation depth (see Fig. 3). The change in effective index (Δn_{eff}) is then given by $(\Delta n_{eff}/n_{eff}) = (\Delta\lambda/\lambda_{pb})$, where n_{eff} (=3.3746) is the effective refractive index of the fundamental TE-like mode of the rib waveguide calculated by the BPM, and $\lambda_{pb} = 1552.89$ nm. b) The temperature change (ΔT) for a given drive power is obtained by using a one-dimensional approximation, assuming that heat in the cavity is conducted to the surrounding Si through the isolation SiO_2 regions

$$\Delta T = R_{th}P_d = \frac{P_d}{\frac{\kappa_{SiO2}S_t}{2L_t} + \frac{\kappa_{SiO2}S_{BOX}}{L_{BOX}} + \frac{\kappa_{SiO2}S_{DBR}}{2L_{DBR}}} \quad (1)$$

where R_{th} is the equivalent thermal resistance of the SiO_2 regions, κ_{SiO2} is the thermal conductivity of SiO_2 (1.4 $Wm^{-1}K^{-1}$), S_t is the area of the cavity surface in contact to a lateral isolation trench L_t is the length of a lateral trench, S_{BOX} is the area of the cavity in contact to the BOX layer, L_{BOX} is the thickness of the BOX layer, S_{DBR} is the area of the cavity surface in contact to a DBR, and L_{DBR} is the length of a DBR. Here, we assume that under dc conditions, the temperature is uniform through the whole cavity due to the high thermal conductivity of Si. From a) and b), we obtain a linear dependence of Δn_{eff} with ΔT with a slope of $+8.7 \times 10^{-5}$ K^{-1}. This dependence is significantly smaller than the reported thermooptic coefficient of Si ($+1.86 \times 10^{-4}$ K^{-1} [2]) and may be due to the existence of free-carrier dispersion effect, which opposes the thermooptic effect.

In Fig. 4, we show the calculated modulation depth, using the estimated $\Delta n_{eff}/\Delta T$, of the fabricated device (triangular dots) at $\lambda_{pb} = 1552.89$ nm as a function of the dissipated power and considering the estimated scattering losses of 7 dB. The calculated modulation depth of a similar device with negligible scattering losses is also shown (circular dots). One can see that if the scattering losses in the device are lowered, the modulation depth is expected to increase to 80% for $P_d = 20$ mW. This modulation can be further increased using a top metal heater, as employed in conventional thermooptic devices [8], to avoid a competing plasma dispersion effect and decrease the dissipated power and the transient response of the device.

IV. Conclusion

We demonstrate a 20-μm-long electrically driven active planar F-P microcavity on Si. The microresonator, which is defined by high-aspect-ratio Si/SiO_2 DBRs, has a high finesse of 11.2. A p-i-n configuration is used to inject current into the cavity region. We show that the effective index of refraction in the cavity is modified due to a thermooptic effect. Due to the high finesse of the cavity, the device shows a modulation depth of 53% for a dissipated power of only 20 mW. If the scattering losses in the device are reduced, the modulation depth is expected to reach 80% for the same power dissipation. Micron size and low power consumption make this device very promising for use in Si-based integrated photonic systems on a chip (PSOC).

Acknowledgment

The device was fabricated at the Cornell NanoScience and Technology Facility (CNF).

References

[1] R. A. Soref, "Silicon-based optoelectronics," *Proc. IEEE*, vol. 81, pp. 1687–1706, Dec. 1993.

[2] G. Cocorullo, M. Iodice, and I. Rendina, "All-silicon Fabry–Pérot modulator based on the termo-optic effect," *Opt. Lett.*, vol. 19, no. 6, pp. 420–422, 1994.

[3] G. V. Treyz, P. G. May, and J.-M. Halbout, "Silicon Mach-Zehnder waveguide interferometers based on the plasma dispersion effect," *Appl. Phys. Lett.*, vol. 59, no. 7, p. 771, 1991.

[4] C. Z. Zhao, E. K. Liu, G. Z. Li, Y. Gao, and C. S. Guo, "Zero-gap directional coupler switch integrated into a silicon-on-insulator for 1.3-μm operation," *Opt. Lett.*, vol. 21, no. 20, p. 1664, 1996.

[5] C. Cocorullo, M. Iodice, I. Rendina, and P. M. Sarro, "Silicon thermooptical micro-modulator with 700 kHz −3 dB bandwidth," *IEEE Photon. Technol. Lett.*, vol. 7, pp. 363–365, Apr. 1995.

[6] C. A. Barrios, V. Almeida, and M. Lipson, "Low-power-consumption short-length and high-modulation-depth silicon electro-optic modulator," *J. Lightwave Technol.*, vol. 21, no. 4, pp. 1089–1098, 2003.

[7] A. G. Rickman, G. T. Reed, and F. Namavar, "Silicon-on-insulator optical rib waveguide loss and mode characteristics," *J. Lightwave Technol.*, vol. 12, pp. 1771–1776, Oct. 1994.

[8] R. L. Espinola, M.-C. Tsai, J. T. Yardley, and R. M. Osgood, "Fast and low-power thermooptic switch on thin silicon-on-insulator," *IEEE Photon. Technol. Lett.*, vol. 15, pp. 1366–1368, Oct. 2003.

All-optical control of light on a silicon chip

Vilson R. Almeida, Carlos A. Barrios, Roberto R. Panepucci & Michal Lipson

School of Electrical and Computer Engineering, Cornell University, Ithaca, New York 14853, USA

Photonic circuits, in which beams of light redirect the flow of other beams of light, are a long-standing goal for developing highly integrated optical communication components[1–3]. Furthermore, it is highly desirable to use silicon—the dominant material in the microelectronic industry—as the platform for such circuits. Photonic structures that bend, split, couple and filter light have recently been demonstrated in silicon[4,5], but the flow of light in these structures is predetermined and cannot be readily modulated during operation. All-optical switches and modulators have been demonstrated with III–V compound semiconductors[6,7], but achieving the same in silicon is challenging owing to its relatively weak nonlinear optical properties. Indeed, all-optical switching in silicon has only been achieved by using extremely high powers[8–15] in large or non-planar structures, where the modulated light is propagating out-of-plane. Such high powers, large dimensions and non-planar geometries are inappropriate for effective on-chip integration. Here we present the experimental demonstration of fast all-optical switching on silicon using highly light-confining structures to enhance the sensitivity of light to small changes in refractive index. The transmission of the structure can be modulated by up to 94% in less than 500 ps using light pulses with energies as low as 25 pJ. These results confirm the recent theoretical prediction[16] of efficient optical switching in silicon using resonant structures.

The difficulty of modulating light using silicon structures arises from the weak dependence of the refractive index and absorption coefficient on the free-carrier concentration[17]. For example, for a 300-μm-long 1.55-μm Mach–Zehnder modulator based on rib waveguides with a mode-field diameter of about 5 μm, a minimum optical pump pulse energy of 2 mJ is needed to modify the real part of the refractive index by $\Delta n = -10^{-3}$ in order to achieve 100% modulation[18]. The absorption due to free carriers under such high powers is also small (16 dB cm^{-1} for a waveguide of rectangular cross-section, 450 nm wide and 250 nm high), which demands a straight waveguide as long as 600 μm in order to achieve a modulation depth of 90% (refs 11, 19). Liu *et al.*[20] have recently demonstrated a high-speed silicon optical modulator based on a MOS (metal–oxide–semiconductor) configuration; this modulator was the first high-speed optical active device on silicon—a critical stepping-stone towards an all-integrated silicon optical chip. However, owing to the weak dependence of the silicon refractive index on the free-carrier concentration, the devices in ref. 20 have relatively large lengths (of the order of millimetres).

To overcome the aforementioned limitations of silicon photonic structures, we have recently proposed the use of highly confined resonant structures for low-power light modulation by enhancing the effect of refractive index change on the transmission response[12]. The results indicate that a refractive index change as small as 10^{-3} can induce a large modulation depth of 80% in a compact 20-μm-long structure. On the basis of these theoretical predictions, we present experimental results on an all-optical gate based on a silicon micrometre-size planar ring resonator, which operates with low pump-pulse energies.

The transmission of a ring resonator, coupled to a waveguide, is highly sensitive to the signal wavelength, and is greatly reduced at wavelengths at which the ring circumference corresponds to an integral number of guided wavelengths. Figure 1 shows a silicon-on-insulator (SOI) ring resonator with 10 μm diameter, patterned by electron-beam lithography and subsequently etched by inductively-coupled-plasma reactive ion etching[21]. Both the silicon waveguide and the ring resonator are channel waveguides with 450-nm-wide by 250-nm-high rectangular cross-sections. The Smart Cut SOI wafer used has a buried 3-μm-thick oxide layer. Figure 2 shows the quasi-TM transmitted spectral response of the structure in Fig. 1. The quasi-TM mode is characterized by the magnetic field being oriented predominantly along the plane of the chip. We see that on-resonance the transmitted power drops by more than 10 dB with respect to that off-resonance. The losses at off-resonance wavelengths are 3.5 dB, which include the fibre-to-waveguide coupling losses and the propagation losses in the 7-mm-long waveguide.

By tuning the effective index of the ring waveguide, the resonance wavelength is modified, which induces a strong modulation of the transmitted signal. Here we use 10-ps pump pulses to inject free carriers through two-photon absorption inside the ring resonator[9], thereby tuning its effective refractive index. The probe and pump beam wavelengths are centred around two adjacent resonances of the ring resonator, $\lambda_{res1} = 1{,}535.6$ and $\lambda_{res2} = 1{,}555.5$ nm (Fig. 2), respectively. The cavity quality-factor values for these resonances are, respectively, $Q_{res1} \approx \lambda_{res1}/\Delta\lambda_{FWHM1} = 3{,}410$ and $Q_{res2} \approx \lambda_{res2}/\Delta\lambda_{FWHM2} = 2{,}290$, where $\Delta\lambda_{FWHM1} = 0.45$ nm and $\Delta\lambda_{FWHM2} = 0.68$ nm are the full-width-at-half-maximum resonance bandwidths; these correspond to cavity photon lifetimes of $\tau_{cav1} = \lambda_{res1}^2/(2\pi c\Delta\lambda_{FWHM1}) = 1.8$ ps and $\tau_{cav2} = \lambda_{res2}^2/(2\pi c\Delta\lambda_{FWHM2}) = 2.8$ ps, respectively, where c is the speed of light in vacuum[22]. Thus, despite the resonant nature of the structure, the temporal response of this ultra-small optical gate can theoretically be as short as a few picoseconds.

The laser source for the pump is a tunable mode-locked optical parametric oscillator, which in turn is pumped by a Ti:sapphire picosecond laser at a 78-MHz repetition rate. The optical parametric oscillator generates 1.5-ps pulses that pass through a Fabry–Perot tunable filter ($\Delta\lambda_{FWHM} = 0.37$ nm) in order to produce the pump beam, which comprises 10-ps pulses with energy of less than 25 pJ coupled to the silicon waveguide input. A tunable continuous-wave laser provides the probe signal. Both pump and probe beams are set to be linearly polarized (quasi-TM) by use of independent polarization controllers. The pump and probe beams are combined by directional couplers, and coupled into the silicon waveguide by an external tapered-lensed fibre and an on-chip fibre-to-waveguide nanotaper coupler[21]. The transmitted probe signal is coupled into a collimator, and separated from the transmitted pump light through a band-pass tunable grating filter ($\Delta\lambda_{FWHM} = 1.4$ nm). The probe signal is detected by a high-speed DC–12 GHz photodetector with a

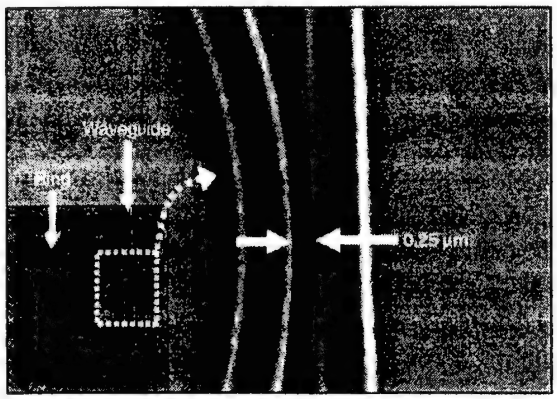

Figure 1 Scanning electron micrograph showing the top view of a ring resonator coupled to a waveguide. Inset shows the whole ring structure.

nominal fall/rise time of 30 ps. A 20-GHz digital sampling oscilloscope is used to record the probe signal.

The temporal responses of the transmitted probe signals are shown in Fig. 3 for two distinct probe wavelengths around λ_{res1}: $\lambda_{probe1} = 1{,}535.2$ nm (below resonance) and $\lambda_{probe2} = 1{,}535.6$ nm (on resonance). These probe wavelengths were tuned relative to the ring resonance in order to maximize the modulation depth by setting the transmission without pump to high and low levels, respectively. An important figure-of-merit for switching is the modulation depth (MD), defined as $MD = (I_{max} - I_{min})/I_{max}$, where I_{max} and I_{min} are, respectively, the maximum and minimum transmitted probe optical power; we measured $MD_{probe1} = 94\%$ for λ_{probe1} and $MD_{probe2} = 91\%$ for λ_{probe2}.

By assuming an instantaneous spectral shift of the spectrum shown in Fig. 2, followed by a simple exponential decay representing the free-carrier lifetime, we obtain from the experimental data a wavelength peak shift of $\Delta\lambda = -0.36$ nm and a relaxation time of $\tau_{fc} = 450$ ps. The measured free-carrier lifetime, much shorter than that in bulk silicon, is not a fundamental limit on the speed; it is due primarily to fast recombination mechanisms on the unpassivated sidewalls of the structures. By manipulating the degree of surface passivation or by using ion implantation[24], the free-carrier lifetime could be further decreased; in this approach, using a pump timescale much shorter than the free-carrier lifetime, the pulse energy required for operating the device remains unaltered since the switching effect occurs before the recombination process becomes significant.

The wavelength peak shift of the ring resonator corresponds to an effective index change of $\Delta n_{eff} = -4.8 \times 10^{-4}$, or equivalently to a refractive index change in the silicon core of $\Delta n_{Si} = -5.2 \times 10^{-4}$. This refractive index change is caused by a free-carrier concentration of $\Delta N = \Delta P = 1.6 \times 10^{17}\,cm^{-3}$. The free-carrier concentration generated in the ring resonator is proportional to the square of the circulating peak pump power. Taking into account the volume of the ring, we estimate that the optical pulse energy absorbed inside the ring resonator in order to excite such a free-carrier concentration is only 0.15 pJ. The remaining pump power, necessary for the two-photon absorption effect, is scattered from the ring. However, this energy could be recycled by using an add/drop configuration, where an additional waveguide is added symmetrically adjacent to the ring. The losses due to the probe absorption[2], estimated from free-carrier concentration, are $\Delta\alpha = 6.9\,cm^{-1}$, significantly lower than the estimated scattering losses in the ring resonator of $\alpha_{ring} = 33.6\,cm^{-1}$. The relatively low absorption losses indicate that the observed modulation is due only to a refractive index change and that thermal effects can be neglected. This is of foremost importance for the application of the proposed device as an all-optical gate, enabling near 100% transmission of the data signal once the gate is open.

The device demonstrated in the present work could be used as a modulator, switch or router, with a time response as low as 100 ps. As a router, the device could route nanosecond-long data for reconfigurable optical interconnects[24]. For such applications, an alternative geometry for the ring resonator, where the ring is coupled to two waveguides, could be used[6]. In this geometry, the incoming data and the control signal are coupled to the input port of the first waveguide (which contains the input port and the through port), whereas the signal output is routed to the second waveguide (the drop port). The device could switch incoming data to either the drop port or the through port, depending respectively on the presence or absence of a control pulse. For such an application, the incoming data stream would be tuned to one of the microring resonances and a control signal would be tuned to an adjacent resonance, as was done in this work.

In order to minimize the effect of the temperature variations on the device performance, strain in the silicon waveguide could be used[25], introduced in the fabrication process by, for example, controlling the overcladding deposition conditions[26]. The introduced strain induces a decrease of the refractive index with temperature, which counterbalances the thermo-optic effect in silicon[25].

The wavelength sensitivity of the device could be decreased by minimizing the size of the ring resonators, which would result in a decrease in Q. According to our three-dimensional finite-difference time-domain simulations, ring resonators with radii as small as 0.9 μm show round-trip bending loss of less than 0.5 dB due to the high index contrast nature of the Si/SiO_2 platform; this is supported by recent experimental results[27]. The average dissipated pump powers required for smaller resonators are similar to those required for larger resonators, in order to achieve the same modulation depth values. This is because although a larger wavelength shift is needed to obtain similar modulation depths in the smaller rings (owing to their lower Q), less pump-pulse energy is needed to obtain similar free-carrier concentrations (owing to their smaller volume).

The device described here is achieved by using the concept of strong light confinement, and is approximately seven orders of magnitude faster than available silicon optical switches[28]. We expect

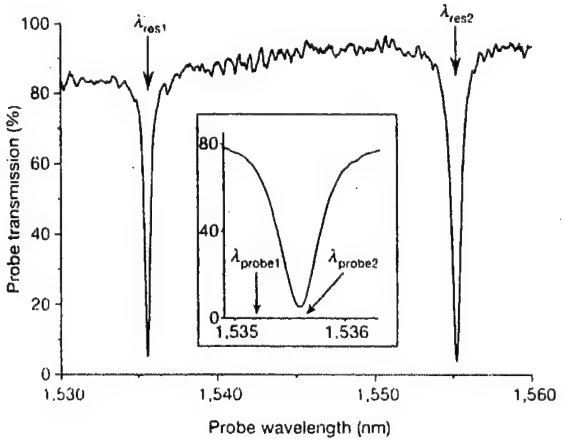

Figure 2 Quasi-TM transmission spectrum of a single-coupled ring resonator in the absence of the optical pump. Inset shows both probe wavelength settings ($\lambda_{probe1} = 1{,}535.2$ nm and $\lambda_{probe2} = 1{,}535.6$ nm) used for characterizing the dynamic response of the switch.

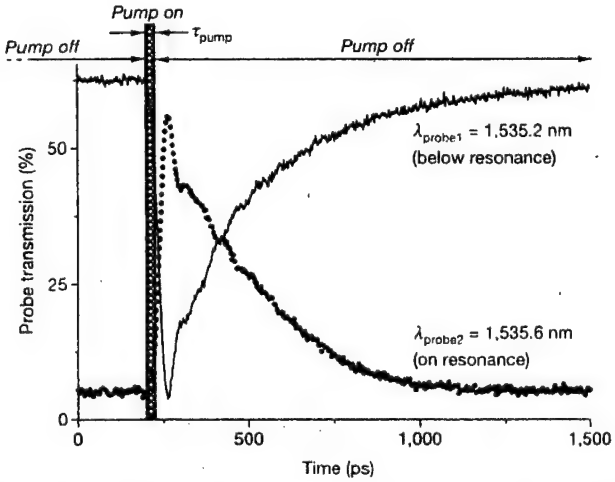

Figure 3 Temporal response of the probe signal to the pump excitation. Transmission for probe wavelengths below resonance (solid line) and on resonance (dotted line) is shown.

that a variety of existing fabrication methods may be used to further improve the speed of the proposed device. The device shown here could form the basis for ultra-high routing bandwidth, by using architectures based on wavelength division multiplexing[29]. □

Received 5 March; accepted 5 August 2004; doi:10.1038/nature02921

1. Tsao, C. Y. Joannopoulos, J. D. & Fan, S. Nonlinear photonic crystal microdevices for optical integration. *Opt. Lett.* **28**, 637–639 (2003).
2. Krauss, T. F. Planar photonic crystal waveguide devices for integrated optics. *Phys. Status Solidi A* **197**, 688–702 (2003).
3. Yablonovitch, E. Photonic crystals: semiconductors of light. *Sci. Am.* **285**, 47–55 (2001).
4. Loncar, M., Doll, T., Vuckovic, J. & Scherer, A. Design and fabrication of silicon photonic crystal optical waveguides. *J. Lightwave Technol.* **18**, 1402–1411 (2000).
5. Wada, K., Tsuan, H. C., Tan, D. R. C. & Kimerling, L. C. On chip interconnection beyond semiconductor roadmap: Silicon microphotonics. *Proc. SPIE* **4870**, 437–443 (2002).
6. Ibrahim, T. A. *et al.* All-optical switching in a laterally coupled microring resonator by carrier injection. *IEEE Photon. Technol. Lett.* **15**, 36–38 (2003).
7. Van, V. *et al.* All-optical nonlinear switching in GaAs–AlGaAs microring resonators. *IEEE Photon. Technol. Lett.* **14**, 74–76 (2002).
8. Leonard, S. W., van Driel, H. M., Birner, A. & Gösele, U. All-optical ultrafast tuning of two-dimensional silicon photonic crystals via free-carrier injection. *Summaries of Papers Presented at the Quantum Electronics and Laser Science Conference. Postconference Technical Digest* 159 (Optical Society of America, Washington DC, 2001).
9. Tan, H. W., van Driel, H. M., Schweizer, S. L., Wehrspohn, R. B. & Gösele, U. Tuning a 2-D silicon photonic crystal using nonlinear optics. *Conf. on Laser and Electro-Optics 2004* Vol. IFD2 (Optical Society of America, Washington DC, 2004).
10. Hache, A. & Bourgeois, M. Ultrafast all-optical switching in a silicon-based photonic crystal. *Appl. Phys. Lett.* **77**, 4089–4091 (2000).
11. Normandin, R., Houghton, D. C. & Simard-Normandin, M. All-optical, silicon based, fiber optic modulator using a near cutoff region. *Can. J. Phys.* **67**, 412–419 (1989).
12. Cucorullo, G. *et al.* Fast infrared light modulation in a-SiH micro-devices for fiber-to-the-home applications. *J. Non-Cryst. Solids* **266–269**, 1247–1251 (2000).
13. Tsang, H. K. *et al.* Optical dispersion, two-photon absorption and self-phase modulation in silicon waveguides at 1.5 μm wavelength. *Appl. Phys. Lett.* **80**, 416–418 (2002).
14. Henari, F. Z., Morgenstern, K., Blau, W. J., Karavanskii, V. A. & Dneprovskii, V. S. Third-order optical nonlinearity and all optical switching in porous silicon. *Appl. Phys. Lett.* **67**, 323–325 (1995).
15. Soref, R. A. & Lorenzo, J. P. Light-by-light modulation in silicon-on-insulator waveguides. *Digest of the OSA Integrated and Guided Wave Optics Topical Meeting* 86–89 (Optical Society of America, Washington DC, 1989).
16. Barrios, C. A., Almeida, V. R. & Lipson, M. Low-power-consumption short-length and high-modulation-depth silicon electrooptic modulator. *J. Lightwave Technol.* **21**, 1089–1098 (2003).
17. Soref, R. A. & Bennett, B. R. Kramers-Kronig analysis of electro-optical switching in silicon. *Proc. SPIE* **704**, 32–37 (1987).
18. Zhao, C. Z., Li, G. Z., Liu, E. K., Gao, Y. & Liu, X. D. Silicon on insulator Mach–Zehnder waveguide interferometers operating at 1.3 μm. *Appl. Phys. Lett.* **67**, 2448–2449 (1995).
19. Stepanov, S. & Ruschin, S. Modulation of light by light in silicon-on-insulator waveguides. *Appl. Phys. Lett.* **83**, 5151–5153 (2003).
20. Liu, A. *et al.* A high-speed silicon optical modulator based on a metal-oxide-semiconductor capacitor. *Nature* **427**, 615–618 (2004).
21. Almeida, V. R., Panepucci, R. R. & Lipson, M. Nanotaper for compact mode conversion. *Opt. Lett.* **28**, 1302–1304 (2003).
22. Verdeyen, J. T. *Laser Electronics*, 3rd edn 153 (Prentice Hall, Upper Saddle River, NJ, 2000).
23. Chin, A., Lee, K. Y., Lin, B. C. & Horng, S. Picosecond photoresponse of carriers in Si ion-implanted Si. *Appl. Phys. Lett.* **69**, 653–655 (1996).
24. Meindl, J. D. *et al.* Interconnect opportunities for gigascale integration. *IBM Res. Dev.* **46**, 245–263 (2002).
25. Weiss, S. M., Molinari, M. & Fauchet, P. M. Temperature stability for silicon-based photonic band-gap structures. *Appl. Phys. Lett.* **83**, 1980–1982 (2003).
26. Cheben, P., Xu, D.-X., Janz, S. & Delâge, A. Scaling down photonic waveguide devices on the SOI platform. *Proc. SPIE* **5117**, 147–156 (2003).
27. Vlasov, Y. A. & McNab, S. J. Losses in single-mode silicon-on-insulator strip waveguides and bends. *Opt. Express* **12**, 1622–1631 (2004).
28. Pardo, F. *et al.* Optical MEMS devices for telecom systems. *Proc. SPIE* **5116**, 435–444 (2003).
29. Miller, D. A. B. Optical interconnects to silicon. *IEEE J. Sel. Top. Quant. Electron.* **6**, 1312–1317 (2000).

Acknowledgements We acknowledge support by the Cornell Center for Nanoscale Systems, funded by the National Science Foundation (NSF), by the Air Force Office of Scientific Research (AFOSR) and by the CS-WDM programme of the Defense Advanced Research Project Agency. V.R.A. acknowledges sponsorship support provided by the Brazilian Defence Ministry. This work was performed in part at the Cornell Nano-Scale Science & Technology Facility (CNF), a member of the National Nanotechnology Infrastructure Network (NNIN) which is supported by the NSF, its users, Cornell University and Industrial Affiliates.

Competing interests statement The authors declare that they have no competing financial interests.

Correspondence and requests for materials should be addressed to M.L. (lipson@ece.cornell.edu).

All-optical switching on a silicon chip

Vilson R. Almeida, Carlos A. Barrios, Roberto R. Panepucci, and Michal Lipson

School of Electrical and Computer Engineering, Cornell University, Ithaca, New York 14853

Mark A. Foster, Dimitre G. Ouzounov, and Alexander L. Gaeta

School of Applied and Engineering Physics, Cornell University, Ithaca, New York 14853

Received June 11, 2004

We present an experimental demonstration of fast all-optical switching on a silicon photonic integrated device by employing a strong light-confinement structure to enhance sensitivity to small changes in the refractive index. By use of a control light pulse with energy as low as 40 pJ, the optical transmission of the structure is modulated by more than 97% with a time response of 450 ps. © 2004 Optical Society of America

OCIS codes: 130.3120, 230.4110, 230.1150, 230.3120.

Photonic integrated circuits that bend, split, couple, and filter light have recently been demonstrated in silicon.[1] However, these structures are usually passive, which means that their optical properties are predetermined by the structure design and thus cannot be modified once fabricated. All-optical switches and modulators have been demonstrated by employing III–V compound materials based on photoexcited free-carrier concentrations resulting from one- or two-photon absorption.[2–4] In silicon, all-optical switching has been demonstrated only by use of extremely high powers[5–10] in large or nonplanar structures in which the modulated light propagates out of plane. Such high powers, large dimensions, and nonplanar structure geometries are inappropriate for effective on-chip integration. The difficulty in modulating light with silicon structures arises from the weak dependence of silicon's refractive index and absorption coefficient on the free-carrier concentration.[11,12] As an example, for a 300-μm-long, 1.55-μm Mach–Zehnder modulator based on rib waveguides with a mode-field diameter of approximately 5 μm, a minimum optical pump-pulse energy of 2 mJ is needed to modify the refractive index by $\Delta n = -10^{-3}$ to achieve 100% modulation.[13] The absorption due to free carriers under such high powers is also small (16 dB/cm for a 450-nm-wide and 250-nm-high rectangular cross-sectional waveguide), which requires a straight waveguide as long as 600 μm to achieve a modulation depth of 90%.[6,14]

We recently proposed the use of high optical confinement in resonant structures for efficient light modulation to overcome the aforementioned limitations of silicon photonic structures[15]; our results indicate that a refractive-index change as small as 10^{-3} can induce a large modulation depth of 80% in a compact 20-μm-long structure. Using these theoretical predictions, here we present experimental results on an all-optical gate based on a silicon micrometer-size planar ring resonator that operates with low pump-pulse energies.

A ring resonator coupled to a single waveguide presents optical transmission that is highly sensitive to the signal wavelength and is greatly reduced at wavelengths in which the ring circumference corresponds to an integer number of guided wavelengths. Figure 1 shows a silicon-on-insulator ring resonator with a 5-μm radius, patterned by electron-beam lithography and subsequently etched by plasma reactive-ion etching[16]; both the waveguide and the ring resonator are channel waveguides with 450-nm-wide by 250-nm-high rectangular cross sections. Figure 2(a) shows the quasi-TM transmitted spectral response of the structure in Fig. 1. The quasi-TM mode is characterized by the magnetic field oriented predominantly along the plane of the chip. On resonance the transmission drops by more than 10 dB with respect to that at off resonance. The losses at off-resonance wavelengths are 3.5 dB, which include the fiber-to-waveguide coupling losses and the propagation losses in the 7-mm-long waveguide. The cavity quality factor is $Q \cong \lambda_0/\Delta\lambda_{\mathrm{FWHM}} = 2290$, where $\lambda_0 = 1555.5$ nm is the resonance wavelength and $\Delta\lambda_{\mathrm{FWHM}} = 0.68$ nm is the resonance FWHM. This quality factor corresponds to a cavity photon lifetime of $\lambda_0^2/(2\pi c\Delta\lambda_{\mathrm{FWHM}}) = 1.8$ ps,[17] where c is the speed of light in vacuum. Therefore, despite the resonant nature of the structure, the temporal response of this ultrasmall optical gate can theoretically be as short as a few picoseconds.

Tuning the effective index of the ring waveguide modifies the resonance wavelength, which induces a strong modulation of the transmitted signal. Here we use femtosecond pump pulses centered at a wavelength of $\lambda_{\mathrm{pump}} = 400$ nm to inject free carriers into the ring resonator and thereby tune its effective refractive

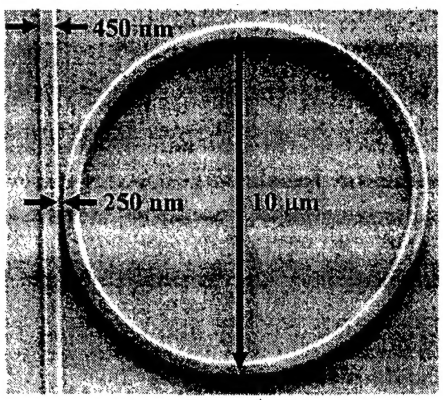

Fig. 1. Scanning electron micrograph showing the top-view of a 5-μm-radius ring resonator coupled to a waveguide.

0146-9592/04/24-03$15.00/0 *(ms #54842aljre)*

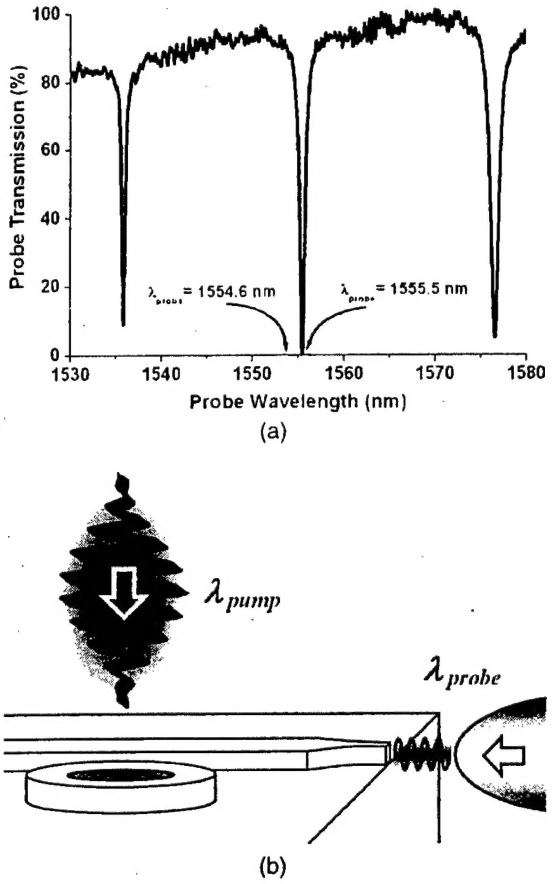

Fig. 2. Device characterization. (a) Quasi-TM spectral response of a singly coupled ring resonator with no optical pump incident on the sample. Both probe wavelengths used in this work for characterizing the dynamic response of the switch are indicated. (b) Schematic of the pump-and-probe setup, showing an in-plane cw optical probe (λ_{probe}) coupled from a tapered-lensed fiber into a nanotaper and an out-of-plane femtosecond optical pump (λ_{pump}).

index. At this wavelength, the strong linear absorption in silicon causes 90% of the photons transmitted into the top silicon layer to be absorbed within a thickness of only 250 nm. After the pulse is absorbed, photoexcited free-carrier electron-hole pairs are generated inside the ring resonators and are subjected to recombination dynamics dictated by the free-carrier lifetime.

Figure 2(b) shows the schematic of the pump-and-probe setup used for characterizing the device, in which the pump laser beam incident on the ring from free space is focused by a lens onto a spot diameter of 14 μm centered on the ring resonator. The laser source for the pump is a mode-locked Ti:sapphire laser that generates 100-fs pulses at 800 nm with 5 nJ of energy at a 80-MHz repetition rate. A β-barium borate crystal is used to generate second-harmonic femtosecond pulses centered at $\lambda_{pump} = 400$ nm. The energy of the pulse incident on the ring resonator plane is less than 40 pJ. A tunable continuous-wave laser provides the probe signal, which is coupled into the silicon waveguide by an external tapered-lensed fiber and an on-chip fiber-to-waveguide nanotaper coupler.[16] The quasi-TM transmitted light is collimated by a lens (N.A. = 0.55), discriminated by a polarizer, and focused into a multimode fiber through a collimator. The probe signal is detected by a high-speed dc 5-GHz photodetector with a nominal fall–rise time of 70 ps. A 20-GHz digital sampling oscilloscope is used to record the probe signal. The temporal response of the transmitted probe signals are shown in Fig. 3 for two distinct probe wavelengths: $\lambda_{probe} = 1554.6$ nm (below resonance) and $\lambda_{probe} = 1555.5$ nm (on resonance).

These probe wavelengths were tuned relative to the ring resonance to maximize the modulation depth when the transmission without the pump was high and low, respectively. The modulation depth is defined as MD = $(I_{max} - I_{min})/I_{max}$, where I_{max} and I_{min} are the maximum and minimum transmitted probe optical power, respectively. We measure MD = 75% for $\lambda_{probe} = 1554.6$ nm and MD = 97% for $\lambda_{probe} = 1555.5$ nm. The measured modulation depth is limited by only the photodetector response time. For a photodetector with a response time of less than 20 ps we expect to measure modulation depths of nearly 100% at both probe wavelengths.

By assuming an instantaneous spectral shift of the spectrum shown in Fig. 2(a), followed by a simple exponential decay representing the free-carrier lifetime, we obtain from the experimental date a wavelength peak shift of $\Delta\lambda = -1.1$ nm and a relaxation time of $\tau_{fc} = 450$ ps. The measured free-carrier lifetime, much shorter than that in bulk silicon, is not a fundamental limit on the speed; it is due primarily to fast recombination mechanisms on the unpassivated sidewalls of the structures. Manipulating the degree of surface passivation or using ion implantation[18] could further reduce the free-carrier lifetime. The wavelength peak shift of the ring resonator corresponds to an effective-index change of $\Delta n_{eff} = -1.45 \times 10^{-3}$ or equivalently to a refractive-index change in the silicon core of $\Delta n_{Si} = -1.6 \times 10^{-3}$. This refractive-index change is caused by a free-carrier concentration

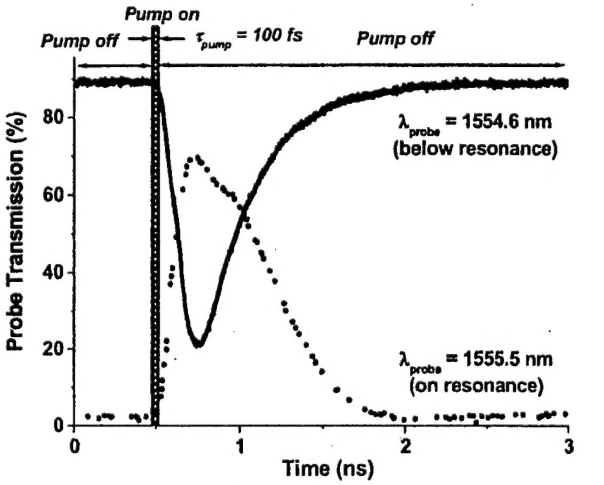

Fig. 3. Temporal response of the probe signal to the pump excitation, showing transmission for probe wavelengths below resonance (solid curve) and on resonance (dotted curve).

of $\Delta N = \Delta P = 4.8 \times 10^{17}$ cm^{-3}. Considering the physical dimensions of the ring resonator, we estimate that the optical pulse energy that needs to be absorbed by the ring resonator to excite such a free-carrier concentration is only 0.9 pJ.

This value is consistent with our estimate that takes into account the energy of the pump pulse incident on the ring, the geometry of the ring resonator, the transverse pump beam profile, and the reflections from the focusing lens and the interfaces in the structure. The losses due to the probe absorption,[2] estimated from the free-carrier concentration are $\Delta\alpha = 6.9$ cm^{-1}, significantly lower than the estimated scattering losses in the ring resonator of $\alpha_{\text{ring}} = 33.6$ cm^{-1}. The relatively low absorption losses indicate that the observed modulation is due only to a refractive-index change and that thermal effects can be neglected. Our calculations predict that a temperature increase of only 2 K is expected for a 2-GHz modulation rate; this has a negligible effect on the all-optical switch performance because the typical time scale of the thermo-optic effect, on the order of a few microseconds,[7] is much longer than that of the device, on the order of 450 ps. The low absorption losses are of foremost importance for the application of the proposed device as an all-optical gate, allowing nearly 100% transmission of the data signal when the gate is open.

The device described here is achieved by use of the concept of strong light confinement and is approximately 7 orders of magnitude faster than available silicon optical switches.[19] We expect that a variety of existing fabrication methods may be used to further improve the speed of the proposed device. The present device could function as an all-optical switch, modulator or router, in applications relevant to optical interconnects. It could form the basis for new interconnect architectures including cabinet-to-cabinet, board-to-board, chip-to-chip, and on-chip architectures, with lower power, less skew, and less jitter relative to the wiring approach of the electrical interconnects.[20,21] In addition, the device shown here could form the basis for ultrahigh interconnection bandwidth, by employing architectures based on wavelength division multiplexing.[21] For logic applications a scheme of optical pumping using the same wavelength as the propagating signal is necessary; this would require the demonstration of efficient two-photon optical mechanisms in silicon.[5]

The authors acknowledge support from the Cornell Center for Nanoscale Systems, through the National Science Foundation (NSF). V. R. Almeida, C. A. Barrios, R. R. Panepucci, and M. Lipson (lipson@ece.cornell.edu) acknowledge support from the Air Force Office of Scientific Research, the Chip-scale Wavelength Division Multiplexing program of the Defense Advanced Research Projects Agency, and the Science and Technology Centers program of the NSF. V. R. Almeida acknowledges sponsorship support provided by the Brazilian Defense Ministry. M. A. Foster, D. G. Ouzounov, and A. L. Gaeta acknowledge support from the Army Research Office and the Air Force Office of Scientific Research. This work was performed in part at the Cornell NanoScale Science & Technology Facility, a member of the National Nanotechnology Infrastructure Network, which is supported by the NSF, its users, Cornell University, and industrial affiliates.

References

1. K. Wada, H. C. Luan, D. R. C. Lim, and L. C. Kimerling, Proc. SPIE **4870,** 437 (2002).
2. T. A. Ibrahim, W. Cao, Y. Kim, J. Li, J. Goldhar, P.-T. Ho, and Chi H. Lee, IEEE Photon. Technol. Lett. **15,** 36 (2003).
3. V. Van, T. A. Ibrahim, K. Ritter, P. P. Absil, F. G. Johnson, R. Grover, J. Goldhar, and P.-T. Ho, IEEE Photon. Technol. Lett. **14,** 74 (2002).
4. T. A. Ibrahim, W. Cao, Y. Kim, J. Li, J. Goldhar, P. T. Ho, and Chi H. Lee, J. Lightwave Technol. **21,** 2997 (2003).
5. S. W. Leonard, H. M. van Driel, J. Schilling, and R. B. Wehrspohn, in *Quantum Electronics and Laser Science (QELS)*, Vol. 57 of OSA Trends in Optics and Photonics Series (Optical Society of America, Washington, D.C., 2001), p. 159.
6. R. Normandin, D. C. Houghton, and M. Simard-Normandin, Can. J. Phys. **67,** 412 (1989).
7. G. Cocorullo, F. G. Della Corte, R. De Rosa, I. Rendina, A. Rubino, and E. Terzini, J. Non-Cryst. Solids **266–269,** 1247 (2000).
8. H. K. Tsang, C. S. Wong, T. K. Liang, I. E. Day, S. W. Roberts, A. Harpin, J. Drake, and M. Asghari, Appl. Phys. Lett. **80,** 416 (2002).
9. F. Z. Henari, K. Morgenstern, W. J. Blau, V. A. Karavanskii, and V. S. Dneprovskii, Appl. Phys. Lett. **67,** 323 (1995).
10. R. A. Soref and J. P. Lorenzo, in *Integrated Guided Wave Optics*, Vol. 4 of 1989 OSA Technical Digest Series (Optical Society of America, Washington, D.C., 1989), p. 86.
11. R. A. Soref and B. R. Bennett, Proc. SPIE **704,** 32 (1987).
12. C. H. Lee, *Picosecond Optoelectronic Devices* (Academic, San Diego, Calif., 1984), Chap. 5.
13. C. Z. Zhao, G. Z. Li, E. K. Liu, Y. Gao, and X. D. Liu, Appl. Phys. Lett. **67,** 2448 (1995).
14. S. Stepanov and S. Ruschin, Appl. Phys. Lett. **83,** 5151 (2003).
15. C. A. Barrios, V. R. Almeida, and M. Lipson, J. Lightwave Technol. **21,** 1089 (2003).
16. V. R. Almeida, R. R. Panepucci, and M. Lipson, Opt. Lett. **28,** 1302 (2003).
17. J. T. Verdeyen, *Laser Electronics*, 3rd ed. (Prentice Hall, Upper Saddle River, N.J., 2000).
18. A. Chin, K. Y. Lee, B. C. Lin, and S. Horng, Appl. Phys. Lett. **69,** 653 (1996).
19. F. Pardo, V. A. Aksyuk, S. Arney, H. Bair, N. R. Basavanhally, D. J. Bishop, G. R. Bogart, C. A. Bolle, J. E. Bower, D. Carr, H. B. Chan, R. A. Cirelli, E. Ferry, R. E. Frahm, A. Gasparyan, J. V. Gates, C. R. Giles, L. Gomez, S. Goyal, D. S. Greywall, M. Haueis, R. C. Keller, J. Kim, F. P. Klemens, P. R. Kolodner, A. Kornblit, T. Kroupenkine, W. Y. Lai, V. Lifton, J. Liu, Y. L. Low, W. M. Mansfield, D. Marom, J. F. Miner, D. T. Neilson, M. A. Paczkowski, C. S. Pai, A. G. Ramirez, D. A. Ramsey, S. Rogers, R. Ryf, R. E. Scotti, H. R. Shea, M. E. Simon, H. T. Soh, H. Tang, J. A. Taylor, K. Teffeau, J. Vuillemin, and J. Weld, Proc. SPIE **5116,** 435 (2003).
20. A. V. Mule, E. N. Glytsis, T. K. Gaylord, and J. D.

Meindl, IEEE Trans. Very Large Scale Integr. (VLSI) Syst. **10,** 582 (2002).

21. D. A. B. Miller, IEEE J. Sel. Top. Quantum Electron. **6,** 1312 (2000).

(ms #54842aljre)